QUANTUM FIELD THEORETICAL METHODS IN MANY BODY SYSTEMS *) **)

J. NIEVES†)

Departamento de Física Teórica and Instituto de Física Corpuscular, Centro Mixto, Universidad de Valencia – Consejo Superior de Investigaciones Científicas, E-46100 Burjassot, Valencia, Spain

Received 15 March 1996

We study the way the nucleon-nucleon interaction is modified inside of a nuclear medium, paying special attention to the spin-isospin channel. Several physical processes which are particularly sensitive to this part of the interaction are reviewed and the importance of the medium corrections to describe their dynamics is analyzed.

Contents

*) Lecture given at the 8th Summer School on Intermediate Energy Physics: "Hadron Dynamics at Low and Intermediate Energies", Prague, July 10–14, 1995.

**) This work was sponsored by CICYT (Spain) research project AEN93-1205 (postdoctoral contract).

†) Permanent address: Departamento de Física Moderna, Universidad de Granada, Granada 18071, Spain.

[1]) This section is based on Ref. 7.

[2]) This section is based on Ref. 16.

[3]) This section is based on Ref. 21.

[4]) This section is based on Refs. 21 and 40–42.

1 Introduction

These lectures pretend to be an exercise on many body quantum field theory by applying basic principles to a variety of physical processes which seem originally rather disconnected, but which, as we will see, share a common factor: the essential role played by the medium renormalization of the vacuum interactions in the correct understanding of their respective dynamics.

In order to follow the lectures, some knowledge of many body theory has been assumed, although some of the concepts are introduced here. Excellent reviews on the topic can be found in Refs. 1–4.

The lectures begin with an analogy, by looking at the way the well known Coulomb interaction is screened in an electron gas. This analogy allows us to introduce concepts like the medium polarization, which will help us to study the way the NN interaction is modified inside of a nuclear medium, leading to the concept of induced interaction, which will play a central role in the rest of the lectures.

We will carefully study the spin-isospin channel of the interaction and search for physical processes which are particularly sensitive to this part of the interaction. In the process we review the theoretical situation of muon capture in nuclei, the problem of the Σ and Λ decay in nuclei and finish with a unified study of pionic atoms and low energy pion-nucleus scattering.

Let us begin with a qualitative discussion, extracted from the excellent book of Fetter and Walecka [1], of the properties of the instantaneous Coulomb interaction in an electron gas. The problem has an obvious resemblance with the modification of the strong interaction in a nuclear medium in which we will be interested in the next sections. One electron inside of an electron gas polarizes the medium (Fig. 1) in such a way that, in a region around it, the negative charges are slightly displaced away from the electron, leaving behind the background charge of the positive ions [1].

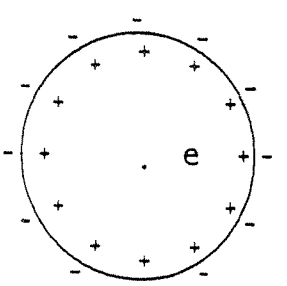

Fig. 1. Polarization of an electron gas due to the presence of an external charge.

As a consequence of this polarization, the photon acquires an effective mass, which leads to the screening of the Coulomb interaction [1]. The original Coulomb interaction is changed to one of shorter range,

$$\frac{1}{4\pi}\frac{1}{r} \to \frac{1}{4\pi}\frac{e^{-\mu(\rho)r}}{r}, \tag{1}$$

where ρ is the electron density of the gas and μ a certain function of it. Note that the effect of the polarization has been to convert the infinite range interaction into one of finite range. The positive charge around one electron, coming from the polarization of the medium, cancels the electron negative charge, and at large distances we see an effective charge zero.

Equation 1 in momentum space is now

$$\frac{1}{\vec{q}^{\,2}} \rightarrow \frac{1}{\vec{q}^{\,2} + \mu^2(\rho)}\,, \tag{2}$$

which corresponds to the instantaneous ($q^0 = 0$) Coulomb piece of the photon propagator and its modification in the electron medium. The physical mechanism for the polarization consists in a transfer of some electrons from occupied states of a Fermi sea to some unoccupied states (Fig. 2), or more technically in producing particle-hole (p-h) excitations. In many body language we express diagramatically the modification of the interaction as shown in Fig. 3.

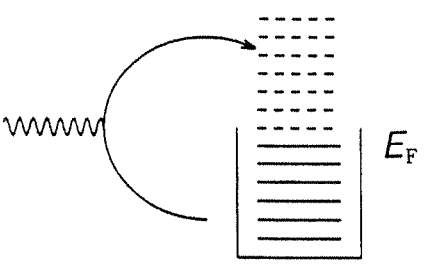

Fig. 2. The energy levels of the Fermi sea are occupied. The photon induces a transition of one electron from one occupied state of the Fermi sea to some unoccupied state.

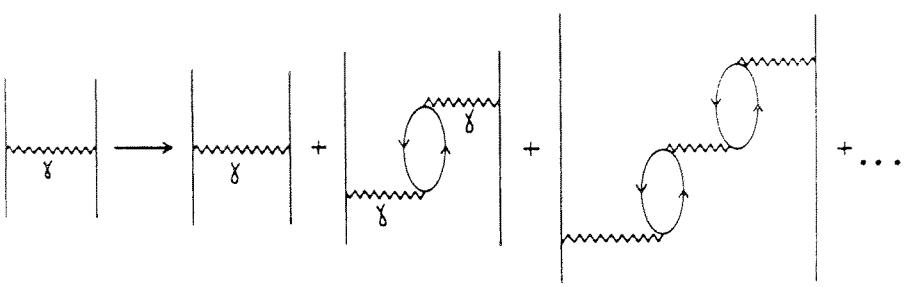

Fig. 3. Modification of the Coulomb interaction due to the polarization of the electron Fermi sea.

The graphs in Fig. 3 are Feynman Many Body diagrams which allow to evaluate the modification of the photon propagator. Hence we can consider the piece of the photon propagator associated to the instantaneous Coulomb part of the interaction (${}_{\mathrm{C}}D_{\mathrm{F}}^{\mu\nu}$) [5], which is now modified in the following way

$$\begin{aligned} {}_{\mathrm{C}}D_{\mathrm{F}}^{\mu\nu}(\vec{q}) &= g^{\mu 0} g^{\nu 0} D_0(\vec{q})\,, \\ D_0(\vec{q}) &= \frac{1}{\vec{q}^{\,2}}\,, \end{aligned}$$

$$\mathrm{i}D_0(\vec{q}) \rightarrow \mathrm{i}D_0(\vec{q}) + \mathrm{i}D_0(\vec{q})(-\mathrm{i}\Pi(q))\,\mathrm{i}D_0(\vec{q}) + \mathrm{i}D_0(\vec{q})(-\mathrm{i}\Pi(q))\,\mathrm{i}D_0(\vec{q})(-\mathrm{i}\Pi(q))\,\mathrm{i}D_0(\vec{q}) + \cdots = \mathrm{i}D(q)\,. \quad (3)$$

Thus we have

$$D(q) = \frac{D_0(\vec{q})}{1 - \Pi(q)D_0(\vec{q})} = \frac{1}{D_0^{-1}(\vec{q}) - \Pi(q)} = \frac{1}{\vec{q}^{\,2} - \Pi(q^0, \vec{q})}\,, \quad (4)$$

where $\Pi(q^0, \vec{q})$ is the component 00 of the photon self-energy due to a single p-h excitation. It is a function of q^0, $\vec{q}$ and the electron density.

The loop in Fig. 3 stands for a p-h excitation as depicted in Fig. 2. The photon would also be renormalized through e^+e^- excitations. One can think of analogies by recalling the picture of the Dirac sea. There, one assumes that all the states of negative energy are filled by electrons. Then a particle-antiparticle excitation is represented (see Fig. 4 left) by a transition of one electron from an occupied state of negative energy to an unoccupied state of positive energy. If now in addition we have

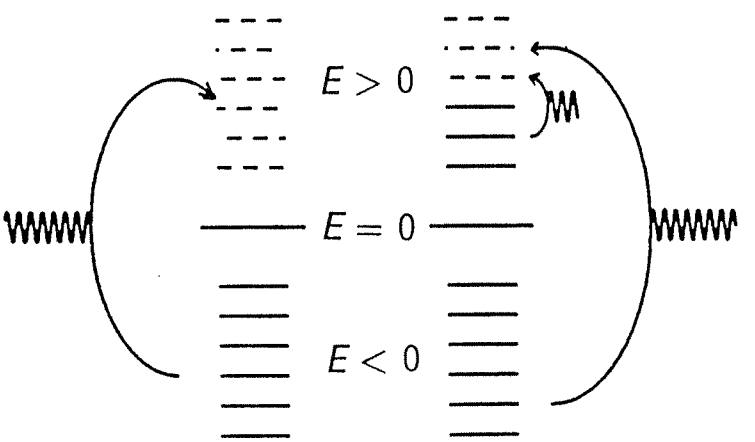

Fig. 4. Left: Representation of the Dirac sea and of e^+e^- excitations. Right: Representation of the p-h excitations (transitions in the positive energy region of the spectrum).

some states of positive energy occupied (states of the Fermi sea), then we can also excite electrons from these occupied states to other unoccupied states of the Fermi sea. These transitions are additional to those from the negative energy states to the positive energy states. In this sense we can now think of the contribution of p-h excitation to the photon self-energy as an additional contribution to the free photon self-energy. This latter one will renormalize the electron mass and charge and the γee coupling, parameters which determine the free electron-electron interaction. Thus the many body corrections renormalize the physical free magnitudes of the theory under study.

For the electromagnetic interaction, given by

$$H_{\mathrm{em}}(x) = -e\,\overline{\Psi}(x)\gamma^\mu\,\Psi(x)A_\mu(x)\,, \quad (5)$$

the Coulomb part of the interaction (zeroth component) in the non-relativistic limit has a trivial limit for the γee vertex, which is just the electron charge e. Thus the self-energy $\Pi(q^0, \vec{q})$ can be evaluated and one finds

$$-\mathrm{i}\Pi(q^0, \vec{q}) = (-\mathrm{i}e)(-\mathrm{i}e)(-2)\int \frac{\mathrm{d}^4k}{(2\pi)^4}\, \mathrm{i}G_0(k)\, \mathrm{i}G_0(k+q)\,, \tag{6}$$

where $(-\mathrm{i}e)$ is the coupling constant times the factor $-\mathrm{i}$ from the perturbative expansion, the minus sign comes because of the fermionic loop, the factor 2 accounts for the two possible spin states of the electron and finally $G_0(k)$ is the electron propagator in a Fermi sea given by [1]

$$G_0(k) = \frac{1 - n(\vec{k})}{k^0 - \epsilon(\vec{k}) + \mathrm{i}\eta} + \frac{n(\vec{k})}{k^0 - \epsilon(\vec{k}) - \mathrm{i}\eta}\,, \tag{7}$$

where $n(\vec{k})$ is the occupation number ($n(\vec{k}) = 0$ for $|\vec{k}| \geq k_\mathrm{F}$, $n(\vec{k}) = 1$ for $|\vec{k}| \leq k_\mathrm{F}$) and $\epsilon(\vec{k})$ is the kinetic energy of the electrons. The k^0 integration in Eq. 6 can be performed in the complex plane and because of the nature of the poles only the first term of $G_0(k)$ times the second one of $G_0(k+q)$, or the second one of $G_0(k)$ times the first one of $G_0(k+q)$ contribute. Thus we get [1]

$$\Pi(q^0, \vec{q}) = e^2 U_\mathrm{e}(q^0, \vec{q})\,, \tag{8}$$

where $U_\mathrm{e}(q^0, \vec{q})$, called the Lindhard function is given by

$$U_\mathrm{e}(q^0, \vec{q}) = 2\int \frac{\mathrm{d}^3k}{(2\pi)^3}\left[\frac{n(\vec{k})(1 - n(\vec{k}+\vec{q}))}{q^0 - \epsilon(\vec{k}+\vec{q}) + \epsilon(\vec{k}) + \mathrm{i}\eta} + \frac{n(\vec{k}+\vec{q})(1 - n(\vec{k}))}{-q^0 + \epsilon(\vec{k}+\vec{q}) - \epsilon(\vec{k}) + \mathrm{i}\eta}\right]. \tag{9}$$

The two terms in Eq. 9 account for the direct and crossed terms of the p-h excitation depicted in Fig. 5.

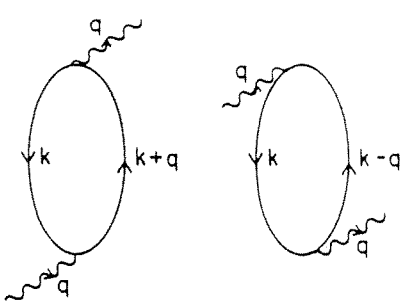

Fig. 5. Direct and crossed terms contributing to the Lindhard function or the photon self-energy.

Note that $U_\mathrm{e}(q)$ can have both real and imaginary parts, which can be calculated by using

$$\frac{1}{k^0 - \epsilon(\vec{k}) + \mathrm{i}\eta} = P\left\{\frac{1}{k^0 - \epsilon(\vec{k})}\right\} - \mathrm{i}\pi\delta(k^0 - \epsilon(\vec{k}))\,, \tag{10}$$

$P\{...\}$ being the principal part, always understood under the integration symbol. Thus, assuming $q^0 > 0$, then only the first term of Eq. 9 gives rise to an imaginary part and we get

$$\mathrm{Im}\, U_{\mathrm{e}}(q) = -2 \int \frac{\mathrm{d}^3 k}{(2\pi)^3} \pi \delta \left[q^0 - \epsilon(\vec{k} + \vec{q}) + \epsilon(\vec{k}) \right] n(\vec{k}) \left[1 - n(\vec{k} + \vec{q}) \right] . \quad (11)$$

The imaginary part of $U_{\mathrm{e}}(q)$ comes from situations in the intermediate states integration, where the particles are placed on shell (momentum conservation in an infinite homogeneous medium is built from the beginning and energy conservation is imposed by the δ function). This is a consequence of a more general theorem, contained in Cutkowski's rules (Ref. 6), which expresses that if we draw a straight line which cuts several lines corresponding to intermediate states in a Feynman diagram, when these lines are placed on shell in the integrations one will get a contribution to the imaginary part of this diagram in the scattering matrix, self-energy, etc...

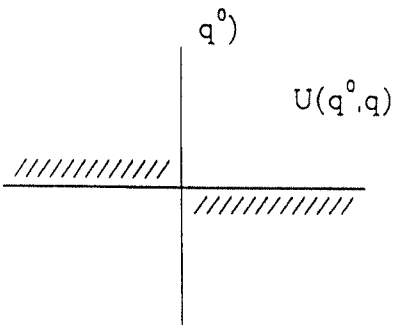

Fig. 6. Analytical structure of the Lindhard function. The dashes represent the analytical cuts. The function $U(q^0, \vec{q})$ is continuous up to the real axis in the first and third quadrant.

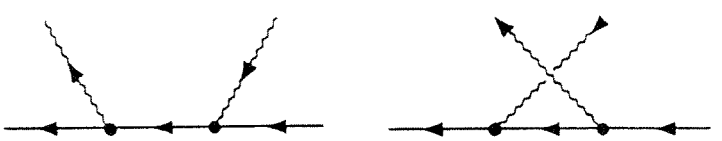

Fig. 7. Direct and crossed diagrams corresponding to the γ–e scattering process.

In the complex q^0 plane, $U(q^0, \vec{q})$ has a continuous set of poles in the fourth quadrant ($q^0 = \epsilon_{\mathrm{par}} - \epsilon_{\mathrm{hole}} - \mathrm{i}\eta$, from the first term of Eq. 9) or in the second quadrant ($q^0 = \epsilon_{\mathrm{hole}} - \epsilon_{\mathrm{par}} + \mathrm{i}\eta$, from the second term of Eq. 9). Hence, $U(q^0, \vec{q})$ has an analytical cut in the second and fourth quadrants as depicted in Fig. 6. The function $U(q)$ has an imaginary part for real values of q^0 situated in the analytical cuts. The integrals in Eq. 9 can be done analytically and analytical expressions for both the real and imaginary parts will be given below.

It is interesting to note that if we open the hole line in Fig. 5 we find the two diagrams that contribute to the photon electron scattering, as shown in Fig. 7.

Thus we can think of the self-energy (8) as an integral of the γe scattering matrix over the occupied states.

2 Virtual meson propagation in nuclei[5])

The introduction in the last section of the propagation of photons through an electron medium simplifies now the discussion of the propagation of pions and other mesons through a nuclear medium. The electric charge of the electron is now substituted by the axial charge of the nucleon, which produces an axial polarization of the medium ([8]). The pion and other mesons will play now the role of the photon as the carriers of the interaction.

2.1 Particle and particle-hole propagators in a Fermi sea: Occupation number and the Lindhard function

Diagramatically the picture for the modification of the pion propagator is identical to that of Fig. 3, by substituting the photons by pions. The πNN effective Hamiltonian, in its non-relativistic form, is given by ($\mu = m_\pi$)

$$\delta H_{\pi\mathrm{NN}}(x) = \frac{f}{\mu}\,\Psi^\dagger(x)\,\sigma_i\,\partial_i\phi^\lambda(x)\,\tau^\lambda\,\Psi(x) \tag{12}$$

with ($f^2/4\pi = 0.08$). $\Psi(x)$ is the nucleon field in the isospin space

$$\Psi^\dagger(x) = \left(\Psi_{\mathrm{p}}^\dagger(x),\,\Psi_{\mathrm{n}}^\dagger(x)\right) \tag{13}$$

with $\Psi_{\mathrm{p,n}}(x)$ the proton and neutron fields and $\phi^\lambda(x)$ the pion field in cartesian isospin basis [9]. In momentum space the πNN vertex for an incoming pion of momentum $\vec{q}$ and isospin λ is given by

$$-\,\mathrm{i}V_{\pi\mathrm{NN}} = \frac{f}{\mu}\vec{\sigma}\vec{q}\,\tau^\lambda. \tag{14}$$

The pion self-energy is now evaluated by summing over the spin and isospin of the particles and we find

$$\Pi(q^0,\vec{q}) = \frac{f^2}{\mu^2}\vec{q}^{\,2}U_{\mathrm{N}}(q^0,\vec{q})\,, \tag{15}$$

omitting the trivial $\delta_{\lambda\lambda'}$ dependence, where

$$U_{\mathrm{N}}(q) = 2U_{\mathrm{e}}(q)\,, \quad (m_{\mathrm{e}} \to m_{\mathrm{N}})\,. \tag{16}$$

Hence formally U_{N} is equal to U_{e} except that we must substitute the electron mass by the nucleon mass. The extra factor two appears since now we also sum over the isospin degrees of freedom of the nucleon. Hence the pion propagator is now modified from its free value:

$$D_0(q) = \frac{1}{q^{0\,2} - \vec{q}^{\,2} - \mu^2 + \mathrm{i}\eta} \;\to\; D(q) = \frac{1}{q^{0\,2} - \vec{q}^{\,2} - \mu^2 - \Pi(q^0,\vec{q})}\,. \tag{17}$$

[5]) This section is based on Ref. 7.

The expression in Eq. 15 for the pion self-energy is however only a first step. Indeed the pion cannot only excite nucleons above the Fermi sea, as implicitly assumed in Eq. 15, but it can also excite the internal degrees of freedom of the nucleon since it is a composite particle made out of quarks. Hence a nucleon can be converted into a Δ, N^*, $\Delta^* \cdots$ Out of these, the Δ plays an important role at intermediate energies because of its lower mass and strong coupling to the πN system.

In an analogous way to Fig. 5 we will now have for the pion self-energy a graphical expression shown in Fig. 8.

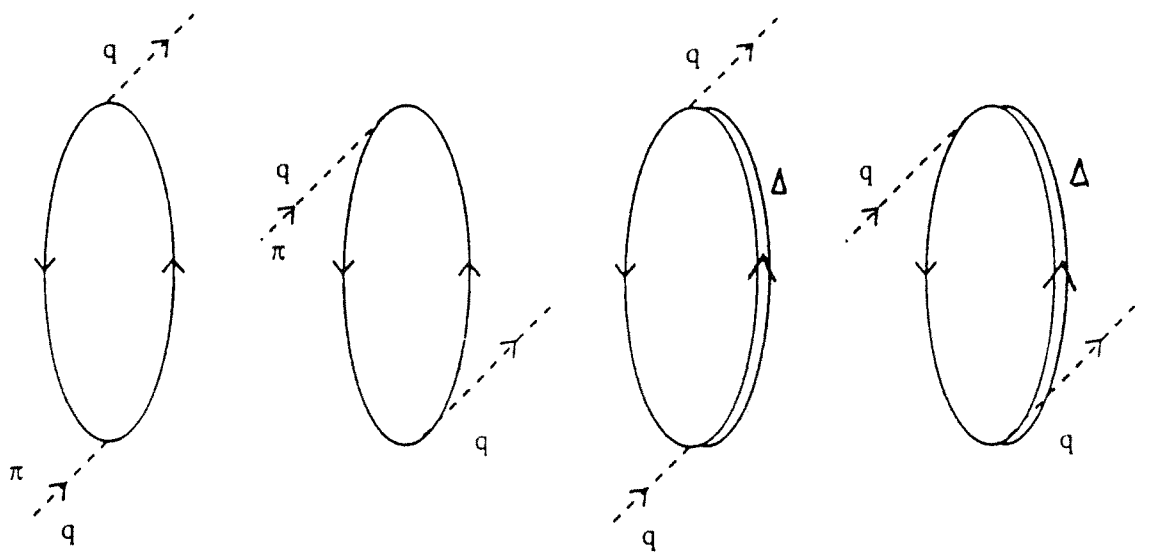

Fig. 8. Diagrams entering the calculation of the pion self-energy in a nuclear medium.

The $\pi N\Delta$ effective Hamiltonian is now given by ($f^{*2}/4\pi = 0.36$)

$$H_{\pi N\Delta} = \frac{f^*}{\mu} \Psi_N^\dagger(x)\, S_i\, \partial_i \phi^\lambda(x)\, T^\lambda\, \Psi_\Delta(x) + \text{h.c.}\,, \tag{18}$$

where $\vec{S}, \vec{T}$ are the transition spin and isospin operators defined by means of the Wigner-Eckart theorem as

$$\left\langle \tfrac{3}{2} M_s \right| S_\nu^\dagger \left| \tfrac{1}{2} m_s \right\rangle = \left(\tfrac{1}{2}, 1, \tfrac{3}{2} | m_s, \nu, M_s\right) \left\langle \tfrac{3}{2} \right| \left| S^\dagger \right| \left| \tfrac{1}{2} \right\rangle \tag{19}$$

with ν the index of a rank one tensor in the spherical basis. The reduced matrix element in Eq. 19 is taken to be the unity, which serves to define the operator[6]) S. A completely analogous expression holds for $T_\lambda^\dagger$.

[6]) A useful expression needed to evaluate the pion self-energy through Δ-h excitation is given by the clousure property

$$\sum_{M_s} S_i \left| \frac{3}{2} M_s \right\rangle \left\langle \frac{3}{2} M_s \right| S_j^\dagger = \delta_{ij} - \frac{1}{3} \sigma_i \sigma_j$$

in cartesian basis.

The pion self-energy for Δ-h excitation, corresponding to the last two diagrams of Fig. 8, can be evaluated by using the same procedure used in the p-h excitation, substituting the vertex $V_{\pi NN}$ by $V_{\pi N\Delta}$ (for the $\pi N \rightarrow \Delta$ transition)

$$-iV_{\pi N\Delta}(q) = \frac{f^*}{\mu}\vec{S}^\dagger \vec{q}\, T^\lambda, \tag{20}$$

and the particle part of the propagator in the Lindhard function by a Δ propagator

$$G_\Delta(k) = \frac{1}{k^0 - w_R - T_\Delta + \frac{1}{2}i\Gamma_\Delta} \tag{21}$$

with $w_R = M_\Delta - M_N$, T_Δ the Δ kinetic energy and Γ_Δ the Δ decay width

$$\frac{\Gamma_\Delta}{2} = \frac{1}{3}\frac{1}{4\pi}\frac{f^{*2}}{\mu^2}\frac{M_N}{\sqrt{s}} q_N^3 \theta(\sqrt{s} - M_\Delta) \tag{22}$$

with q_N the πN c.m. momentum for the decay of a Δ of energy q^0 and $\sqrt{s}$ the c.m. energy of this system.

Note that there is no Fermi sea of Δ resonances and hence the Δ propagator does not have the hole part.

With these ingredients, the pion self-energy now reads

$$\Pi(q^0, \vec{q}) = \frac{f^2}{\mu^2}\vec{q}^2 U(q^0, \vec{q}) \tag{23}$$

with

$$U(q) = U_N(q) + U_\Delta(q) \tag{24}$$

and

$$U_\Delta(q) = -i\left(\frac{4}{3}\right)^2\left(\frac{f^*}{f}\right)^2 \int \frac{d^4k}{(2\pi)^4}\left[G^0(k)G_\Delta(k+q) + G^0(k)G_\Delta(k-q)\right]. \tag{25}$$

Defining the dimensionless variables

$$\nu = \frac{q^0 m}{k_F^2}, \qquad \hat{q} = \frac{q}{k_F}, \tag{26}$$

we have ($m = M_N$) [7]

$$U_N(\nu, \hat{q}) = \frac{mk_F}{\pi^2}\left\{-1 + \frac{1}{2\hat{q}}\left[1 - \left(\frac{\nu}{\hat{q}} - \frac{\hat{q}}{2}\right)^2\right]\ln\frac{\nu/\hat{q} - \hat{q}/2 + 1}{\nu/\hat{q} - \hat{q}/2 - 1}\right.$$
$$\left. - \frac{1}{2\hat{q}}\left[1 - \left(\frac{\nu}{\hat{q}} + \frac{\hat{q}}{2}\right)^2\right]\ln\frac{\nu/\hat{q} + \hat{q}/2 + 1}{\nu/\hat{q} + \hat{q}/2 - 1}\right\} \tag{27}$$

for complex values of q^0. For real values of q^0, Eq. 27 provides the real part of $U_{\rm N}(q)$ by taking the absolute value of the arguments of the ln function. In this latter case we also have

$$\mathrm{Im}\, U_{\rm N}(\nu,\hat{q}) \;=\; \frac{-2mk_{\rm F}}{4\pi\hat{q}}\left[1-\left(\frac{|\nu|}{\hat{q}}-\frac{\hat{q}}{2}\right)^2\right] \tag{28}$$

for $\hat{q}>2$ and $\frac{1}{2}\hat{q}^2+\hat{q}\geq|\nu|\geq\frac{1}{2}\hat{q}^2-\hat{q}$ or $\hat{q}<2$ and $\frac{1}{2}\hat{q}^2+\hat{q}\geq|\nu|\geq\hat{q}-\frac{1}{2}\hat{q}^2$,

$$\mathrm{Im}\, U_{\rm N}(\nu,\hat{q}) \;=\; -\frac{mk_{\rm F}}{\pi\hat{q}}|\nu| \tag{29}$$

for $\hat{q}<2$ and $0\leq|\nu|\leq\hat{q}-\frac{1}{2}\hat{q}^2$, and $\mathrm{Im}\, U_{\rm N}(\nu,\hat{q})=0$ otherwise.

On the other hand, U_Δ is given by

$$\begin{aligned} U_\Delta(q^0,\vec{q}) \;=\; & \left(\frac{4}{3}\frac{f^*}{f}\frac{k_{\rm F}}{2\pi}\right)^2\frac{1}{b^3}\left[b(a+a')+\frac{b^2-a^2}{2}\ln\frac{a+b}{a-b}\right.\\ & \left.+\frac{b^2-a'^2}{2}\ln\frac{a'+b}{a'-b}\right], \end{aligned} \tag{30}$$

where

$$\begin{aligned} b \;&=\; \frac{|\vec{q}|}{M_\Delta}\,,\\ a \;&=\; \frac{1}{k_{\rm F}}\left(q^0-\hat{w}_R(q^0)-\frac{\vec{q}^{\,2}}{2M_\Delta}\right),\\ a' \;&=\; \frac{1}{k_{\rm F}}\left(-q^0-\hat{w}_R(-q^0)-\frac{\vec{q}^{\,2}}{2M_\Delta}\right), \end{aligned}$$

$$\hat{w}_R(q^0) \;=\; w_R = M_\Delta - M_{\rm N}\,, \qquad q^0\epsilon C\,,$$

$$\hat{w}_R(q^0) \;=\; w_R - \mathrm{i}\frac{\Gamma_\Delta(q^0)}{2}\,, \qquad q^0\epsilon R\,. \tag{31}$$

For real values of q^0 for which $\hat{w}_R(q^0)$ is real the arguments in the logarithms must be substituted by their absolute values.

2.2 Induced spin-isospin nucleon-nucleon interaction in a nuclear medium

By analogy to Fig. 7, the model of Fig. 8 implies an assumption for the πN scattering matrix which is given in Fig. 9.

The model of Fig. 9, which contains the nucleon and Δ poles and their crossed terms, accounts for the p-wave of the πN scattering matrix. The s-wave part gives only a small correction for cases where the momentum is not too small. For the case of pionic atoms, which we will study below, the s-wave must be however taken into account.

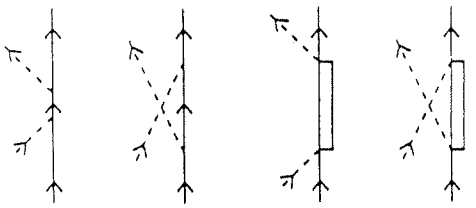

Fig. 9. Model for the πN scattering amplitude implicit in the diagrams of Fig. 8.

The series of Eq. 3 implicitly assumes that a photon (a pion here) propagates in between two particle-hole excitations. It is well known that one pion exchange only accounts for the long range part of the NN interaction, and that at short distances a repulsive force should also be included. The repulsive short range part of the interaction will modify the pion exchange by cutting its contribution to the interaction at short distances. In many problems which are selective to the pionic part of the NN interaction one is only selecting the exchange of a $T = 1$ object, for which the ρ-meson will also play some role. On the other hand, in the propagation of a pion, in those iterated diagrams where more than one p-h excitation occur, the ρ exchange, modified by the effect of short range correlations, plays also some role. For this reason it is customary to talk about the spin-isospin part of the interaction (Refs. 7 and 10).

The ρ meson coupling to the nucleon $V_{\rho\mathrm{NN}}$ is given, in the non-relativistic limit, by

$$H_{\rho\mathrm{NN}}(q) = \mathrm{i}\frac{f_\rho}{m_\rho}(\vec{\sigma} \times \vec{q})\vec{\epsilon}\tau^\lambda\,, \tag{32}$$

where $\vec{\epsilon}$ is the ρ meson polarization vector. Similarly the $\rho\Delta$N coupling for the $\rho\mathrm{N} \rightarrow \Delta$ transition is given by

$$H_{\rho\mathrm{N}\Delta}(q) = \mathrm{i}\frac{f^*_\rho}{m_\rho}(\vec{S}^\dagger \times \vec{q})\,\vec{\epsilon}\,T^\lambda \tag{33}$$

with

$$\begin{aligned} C_\rho &= \frac{f_\rho^2/m_\rho^2}{f^2/\mu^2} \approx 2\,, \\ \frac{f^*_\rho}{f_\rho} &= \frac{f^*}{f}\,. \end{aligned} \tag{34}$$

The short range repulsion, assumed independent of spin-isospin, is attributed to the exchange of the ω-meson in the meson exchange language, although some pictures based on the bag model generate the repulsion from the antisymmetry of the quarks when the two bags overlap (Refs. 11 and 12).

With the couplings πNN and ρNN of Eqs. 14 and 32 we can write the NN potential due to one pion or one ρ-meson exchange

$$-\mathrm{i}V_\pi(q) = \frac{f}{\mu}\vec{\sigma}\vec{q}\tau^\lambda \frac{\mathrm{i}}{\mathrm{q}^{0\,2} - \vec{\mathrm{q}}^{\,2} - \mu^2 + \mathrm{i}\epsilon}\frac{f}{\mu}\vec{\sigma}(-\vec{q})\tau^\lambda\,,$$

$$V_\pi(q) = \frac{f^2}{\mu^2}\frac{\vec{q}^{\,2}}{q^{0\,2}-\vec{q}^{\,2}-\mu^2+\mathrm{i}\epsilon}\hat{q}_i\hat{q}_j\sigma_i^{(1)}\sigma_j^{(2)}\vec{\tau}^{(1)}\vec{\tau}^{(2)}, \tag{35}$$

where the short distance repulsion in coordinate space has still to be implemented and $\hat{q}_i = q_i/|\vec{q}|$.

Analogously when summing over the intermediate ρ polarization

$$\begin{aligned} V_\rho(q) &= \frac{f_\rho^2}{m_\rho^2}\frac{(\vec{\sigma}\times\vec{q})(\vec{\sigma}\times\vec{q})}{q^{0\,2}-\vec{q}^{\,2}-m_\rho^2+\mathrm{i}\epsilon}\vec{\tau}\vec{\tau} \\ &= \frac{f_\rho^2}{m_\rho^2}\frac{\vec{q}^{\,2}}{q^{0\,2}-\vec{q}^{\,2}-m_\rho^2+\mathrm{i}\epsilon}(\delta_{ij}-\hat{q}_i\hat{q}_j)\sigma_i^{(1)}\sigma_j^{(2)}\vec{\tau}^{(1)}\vec{\tau}^{(2)}, \end{aligned} \tag{36}$$

$V_\pi(q) + V_\rho(q)$ provides the spin-isospin part of the NN interaction in the meson exchange model.

We can observe that $V_\pi(q)$ is of a longitudinal type, $\hat{q}_i\hat{q}_j$, while $V_\rho(q)$ is of a transverse type, $(\delta_{ij} - \hat{q}_i\hat{q}_j)$. These two operators are mutually orthogonal.

In addition we must include vertex form factors to account for the off shell mesons. We include a monopole form factor per vertex of the type

$$F_i(q^0,\vec{q}) = \frac{\Lambda_i^2 - m_i^2}{\Lambda_i^2 - q^2}, \tag{37}$$

with $\Lambda_\pi = 1200\,\mathrm{MeV}$ and $\Lambda_\rho = 2500$ MeV (Ref. 13).

With all these ingredients, we are now in position to evaluate the G-matrix. We could think that the hard core is produced by a strong repulsive spin-isospin independent force and we can use the results of Brown and Jackson (Ref. 14) to construct the G-matrix. Thus, we find that if the potential is split into a "weak" spin-isospin dependent part, V_ω, and a "strong" spin-isospin independent part, $V_{\rm s}$,

$$V = V_{\rm s} + V_\omega, \tag{38}$$

the G-matrix is given by

$$G = G_{\rm s} + \Omega_{\rm s}^\dagger V_\omega \Omega_{\rm s} + \ldots, \tag{39}$$

where $G_{\rm s}$ is the G-matrix for the spin-isospin independent part of the interaction constructed with $V_{\rm s}$ alone and $\Omega_{\rm s}^\dagger$, $\Omega_{\rm s}$ are wave operators which in the case of a short-range repulsive potential can be approximated by a local correlation function due to the short range repulsive part. Equation 39 then separates the G-matrix into a spin-isospin independent part and one which is spin-isospin dependent. This last piece will be found by multiplying the spin-isospin dependent potential by the correlation function. This is the procedure followed in Refs. 3 and 7, where an easy analytical correlation function in coordinate space (which vanishes as $r \to 0$ and goes to 1 as $r \to +\infty$) of the type $g(r) = 1 - j_0(q_c)$ with $q_c \approx m_\omega \approx 770\,\mathrm{MeV}$ is

assumed. One can then find the corresponding modification of the potential in the momentum space and thus the modified $\pi + \rho$ interaction reads now

$$\begin{aligned}\hat{V}_{\mathrm{s-i}}(q) &= \left(a\delta_{ij} + b\frac{q^i q^j}{\vec{q}^2}\right)\sigma_i^{(1)}\sigma_j^{(2)}\vec{\tau}^{(1)}\vec{\tau}^{(2)} \\ &= \left[V_{\mathrm{t}}\left(\delta_{ij} - \frac{q^i q^j}{\vec{q}^2}\right) + V_{\mathrm{l}}\frac{q^i q^j}{\vec{q}^2}\right]\sigma_i^{(1)}\sigma_j^{(2)}\vec{\tau}^{(1)}\vec{\tau}^{(2)} \qquad (40)\end{aligned}$$

with $V_{\mathrm{t}}(q)$ and $V_{\mathrm{l}}(q)$ given by

$$\begin{aligned}V_{\mathrm{t}}(q) &= \frac{f^2}{\mu^2}\left[\vec{q}^2 D_0^{\rho}(q)F_{\rho}^2(q)C_{\rho} - \frac{q_c^2}{3}\hat{D_0}^{\pi}(q)\hat{F_{\pi}}^2(q)\right. \\ &\quad \left. - \left(\vec{q}^2 + \frac{2}{3}q_c^2\right)\hat{D_0}^{\rho}(q)\hat{F_{\rho}}^2(q)C_{\rho}\right], \\ V_{\mathrm{l}}(q) &= \frac{f^2}{\mu^2}\left[\vec{q}^2 D_0^{\pi}(q)F_{\pi}^2(q) - \left(\vec{q}^2 + \frac{q_c^2}{3}\right)\hat{D_0}^{\pi}(q)\hat{F_{\pi}}^2(q)\right. \\ &\quad \left. - \frac{2q_c^2}{3}\hat{D_0}^{\rho}(q)\hat{F_{\rho}}^2(q)C_{\rho}\right]. \qquad (41)\end{aligned}$$

$D_0^{\pi}(q)$, $D_0^{\rho}(q)$ are the pion or ρ - meson propagators and $\hat{D_0}, \hat{F}$ the propagators or form factors by substituting $\vec{q}^2$ by $\vec{q}^2 + q_c^2$. We call the interaction in Eq. 40 the nucleon effective interaction.

The second form in Eq. 40 is quite useful because it separates the interaction into a transverse piece, the V_{t} term, and a longitudinal piece, the V_{l} term.

Because we take $C_{\rho} = C_{\rho}^*$, $\Lambda_{\pi,\rho}^* = \Lambda_{\pi,\rho}$ the potential of Eq. 40 describes also the interactions $\Delta\mathrm{N} \rightarrow \mathrm{NN}$, $\mathrm{NN} \rightarrow \Delta\mathrm{N}$, $\Delta\mathrm{N} \rightarrow \Delta\mathrm{N}$ and $\Delta\Delta \rightarrow \mathrm{NN}$ in the vacuum and inside of the nuclear medium respectively, by means of the following replacements:

$$\frac{f}{\mu}\sigma\tau \rightarrow \frac{f^*}{\mu}S^{(\dagger)}T^{(\dagger)}. \qquad (42)$$

The interaction in Eq. 40 acts now between the p-h or Δ-h excitations (the different coupling constant for the $\pi\mathrm{N}\Delta$ is incorporated in the Lindhard function, U_{Δ}). Hence ultimately the picture for the spin-isospin dependent part of the interaction, by accounting also for the propagation of the mesons through the medium, will be, by analogy to Fig. 3, the one shown in Fig. 10.

The series implicit in Fig. 10 can be easily summed up by using the orthogonality between the longitudinal and transverse modes of the interaction.

Thus, one finds two (longitudinal and transverse) geometrical series, which do not interfere

$$\begin{aligned}&\left[\hat{V}_{ij}(q) + \hat{V}_{ik}(q)U(q)\hat{V}_{kj}(q) + \hat{V}_{ik}(q)U(q)\hat{V}_{km}(q)U(q)\hat{V}_{mj}(q) + \ldots\right]\sigma_i^{(1)}\sigma_j^{(2)}\vec{\tau}^{(1)}\vec{\tau}^{(2)} \\ &= \left[\frac{V_{\mathrm{t}}(q)}{1 - U(q)V_{\mathrm{t}}(q)}\left(\delta_{ij} - \frac{q_i q_j}{\vec{q}^2}\right) + \frac{V_{\mathrm{l}}(q)}{1 - U(q)V_{\mathrm{l}}(q)}\frac{q_i q_j}{\vec{q}^2}\right]\sigma_i^{(1)}\sigma_j^{(2)}\vec{\tau}^{(1)}\vec{\tau}^{(2)}. \qquad (43)\end{aligned}$$

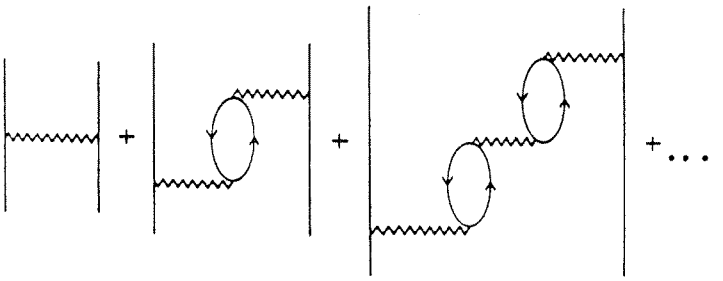

Fig. 10. Picture for the induced spin-isospin interaction in a nuclear medium. The wavy line stands now for the interaction of Eq. 40.

The interaction in Eq. 43 is called in the literature the induced interaction (Ref. 15).

Very often in the literature one uses other expressions for V_l, V_t. The most widely used, in terms of the Landau-Migdal parameter g', can be obtained from Eq. 41 in the limit $|\vec{q}| \ll q_c$

$$\begin{aligned} V_\mathrm{l}(q) &\approx \frac{f^2}{\mu^2}[\vec{q}^{\,2} D_0^\pi(q) F_\pi^2(q) + g'] \,, \\ V_\mathrm{t}(q) &\approx \frac{f^2}{\mu^2}[\vec{q}^{\,2} D_0^\rho(q) F_\rho^2(q) C_\rho + g'] \end{aligned} \tag{44}$$

with

$$g' = -\frac{q_c^2}{3}\hat{D_0}^{\pi}(q)\hat{F_\pi}^{2}(q) - \frac{2}{3}q_c^2\hat{D_0}^{\rho}(q)\hat{F_\rho}^{2}(q)C_\rho \,. \tag{45}$$

This expression gives $g' \approx 0.6$. Accepted values of g' would range from $g' \approx 0.6$ to 0.8.

In the problems which we will study in the next sections $V_\mathrm{t}(q) > 0$, $\mathrm{Re}\, U(q) < 0$, $V_\mathrm{l}(q) < 0$. Thus one finds a decrease of the transverse mode (quenching) and an increase (enhancement) of the longitudinal one (Ref. 7). The net effect of considering the whole induced interaction instead of the bare one depends on the kinematical conditions (range of q) and the weight given to the transverse and longitudinal parts in Eq. 43.

3 Muon capture in nuclei[7])

In this section we review the problem of total muon capture in nuclei from an unconventional point of view. From the early days of Primakoff [17] the subject has attracted much interest [18, 19], since this reaction has been used traditionally to extract information on the value of the pseudoscalar coupling constant [18–20]. The usual approach consists in performing the non-relativistic approximation in the transition operators, neglecting the nucleon-momentum, taking an average nuclear excitation energy [17–19], and then doing a closure sum over the final nuclear states,

[7]) This section is based on Ref. 16.

in some cases improved by means of sum-rule approaches [20]. The final results are then obtained after the evaluation of non-trivial two-body matrix elements in the ground state of the nucleus.

Another approximation traditionally used, to take into account the fact that a muon penetrating into the nucleus does not experience the full charge Z but only the charge included within its orbit, is the use of the effective charge, $Z_{\rm eff}$, which introduces a non-negligible source of error in the calculation since the capture rate is proportional to $Z_{\rm eff}^4$ and certain approximations are involved in its evaluation. In addition there are strong nuclear renormalization effects which are very important and deserve special attention. Thus the traditional method is subject to different (and difficult to control) sources of theoretical uncertainties [16].

The approach of Ref. 16, which we will follow here, avoids all of these problems and provides a highly accurate method to evaluate the total capture rate in nuclei. The method consists in evaluating the capture rate of a muon in a Fermi sea of neutrons and protons (we will see that the only relevant nuclear information needed is the neutron and proton densities of the nuclear ground state, which will be taken from experiment to minimize errors). The calculation can be done exactly in a relativistic framework going beyond the closure sum or the sum rule approach. With the neutrino energy as a variable of integration, the pion pole structure of the pseudoscalar term is kept in the calculations making thus more reliable the information extracted, from this process, about the pseudoscalar coupling.

The step from infinite matter to finite nuclei is done by means of the local density approximation, which turns out to be highly accurate in this case, given the very weak q dependence of the matrix elements involved, which makes the transition of very short range [16]. The infinite matter calculation provides the muon width as a function of $\rho_{\rm p,n}$, the neutron and proton densities, then one assumes $\rho_{\rm p,n} \rightarrow \rho_{\rm p,n}(r)$ and fold this functional with the muon density distribution in the 1s state of the muon atom, from which the capture takes place and avoiding in this way the use of the concept of $Z_{\rm eff}$. In addition effects due to strong nuclear renormalization in the operators and due to binding energies of the muons are also taken into account. We will pay here a special attention to the effects due to the nuclear renormalization (main objective of these lectures) in medium and heavy nuclei, and we will see how this renormalization reduces the capture rates in about of a factor two from the results without renormalization.

3.1 Muon capture rate in infinite matter

We start from the basic Lagrangian for the $\mu^- {\rm p} \rightarrow {\rm n}\nu_\mu$ reaction depicted in Fig. 11:

$$L(x) = \frac{G_{\rm F}}{\sqrt{2}} J^\alpha(x) L_\alpha^\dagger(x) \tag{46}$$

with L_α, J^α the leptonic and hadronic currents respectively and $G_{\rm F}$ the Fermi constant ($G_{\rm F}/(\hbar c)^3 = 1.166 \times 10^{-5}\,{\rm GeV}^{-2}$). The matrix elements of the leptonic

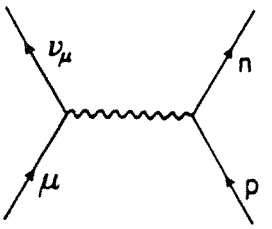

Fig. 11. Diagram for $\mu^- \mathrm{p} \to \mathrm{n}\nu_\mu$ process.

and hadronic currents between spinors give

$$L_\alpha(x) \to \bar{u}_\nu(p_\nu)\gamma_\alpha(1-\gamma_5)u_\mu(p_\mu)\,,$$

$$J^\alpha(x) \to \bar{u}_\mathrm{n}(p_\mathrm{n})\left(g_\mathrm{V}\gamma^\alpha + \mathrm{i}\frac{g_\mathrm{M}}{2m_\mathrm{p}}\sigma^{\alpha\beta}q_\beta + g_\mathrm{A}\gamma^\alpha\gamma_5 + \frac{g_\mathrm{P}}{m_\mu}q^\alpha\gamma_5\right)u_\mathrm{p}(p_\mathrm{p})\,, \quad (47)$$

where we follow the Itzykson and Zuber [6] convention for the γ matrices, with $p_{\mathrm{n,p},\nu,\mu}$ the neutron, proton, neutrino, muon four vectors, $q = p_\mathrm{n} - p_\mathrm{p}$ and g_V, g_M, g_A, g_P the vector, magnetic, axial-vector and pseudoscalar couplings constants respectively, including a form factor dependent on q^2. The values of the coupling constants and the expressions for the form factors can be seen in Ref. 16.

The width of a muon in the infinite Fermi sea of protons and neutrons with $N \neq Z$, due to a single p-h excitation (Fig. 12) is given by[8]), in the Itzykson and Zuber convention [6], as

$$\Gamma = -2\int \frac{\mathrm{d}^3p_\nu}{(2\pi)^3}\frac{m_\mu}{E_\mu}\frac{m_\mathrm{p}}{E_\mathrm{p}}\frac{m_\mathrm{n}}{E_\mathrm{n}}\overline{\sum}\sum|T|^2\mathrm{Im}\,\bar{U}(p_\nu - p_\mu)\,, \quad (48)$$

where T denotes the T-matrix for the $\mu^- \mathrm{p} \to \mathrm{n}\nu_\mu$ process averaged over the Fermi sea (the full expression for $\overline{\sum}\sum|T|^2$ can be found in Ref. 16) and $\bar{U}$ is the Lindhard function (see Eq. 16) for the particle hole excitation of Fig. 12 in asymmetric nuclear matter and is given by

$$\bar{U}(p_\mu - p_\nu) = 2\int \frac{\mathrm{d}^3p}{(2\pi)^3}\frac{n_1(\vec{p})[1-n_2(\vec{p}+\vec{p}_\mu-\vec{p}_\nu)]}{E_\mu - E_\nu + E_\mathrm{p}(\vec{p}) - E_\mathrm{n}(\vec{p}+\vec{p}_\mu-\vec{p}_\nu) + \mathrm{i}\epsilon}\,, \quad (49)$$

where $n_{1,2}(\vec{p})$ are the occupation numbers in the Fermi sea of protons and neutrons respectively[9]).

Equation 48 provides the muon capture width as a function of $k_{\mathrm{F,p}}$ and $k_{\mathrm{F,n}}$, the proton and neutron Fermi momenta or equivalently ρ_p and ρ_n, the proton and neutron densities of the medium ($\rho_{\mathrm{p,n}} = k^3_{\mathrm{F,p,n}}/3\pi^2$).

[8]) Note that Γ is essentially given by the imaginary part of the μ self-energy diagram depicted in Fig. 12, when the ph excitation and the outgoing neutrino are put on shell. Up to some kinematical corrections, this imaginary part is given by the imaginary part of the Lindhard function $\bar{U}(p_\nu - p_\mu)$, which accounts for the ph excitation, and by $\overline{\sum}\sum|T|^2$ which accounts for transition squared operator [16].

[9]) Note that in Eq. 49 the second term of Eq. 9 has not been included because it does not provide imaginary part for $q^0 = E_\mu - E_\nu > 0$.

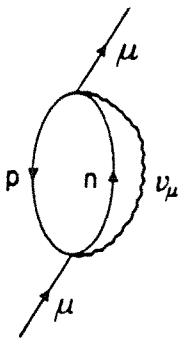

Fig. 12. Many-body Feynman diagram for the muon self-energy related to the $\mu^- \mathrm{p} \rightarrow \mathrm{n}\nu_\mu$ process.

3.2 Strong renormalization effects

The dominant contribution, ($\approx 80\%$), to the process comes from the term proportional to g_{A}^2 in $\overline{\sum} \sum |T|^2$. The non-relativistic reduction of the axial-vector term in the nucleon current is of the type $g_{\mathrm{A}} \sigma^i \tau^\lambda$. We know (see section 2.2) that this external source has the virtue of polarizing the axial charge of the nuclear medium which can produce an important renormalization of the capture rate. Microscopically we can depict the situation by saying that the Feynman diagram of Fig. 12 is now modified to include the series of diagrams implicit in Fig. 13, where the wavy line stands for the spin-isospin p-h or Δ-h interaction, $\hat{V}_{\mathrm{s-i}}$ defined in Eq. 40 for the p-h–p-h interaction case, or a similar one for the case of p-h–Δ-h or Δ-h–Δ-h interactions by means of the replacements in Eq. 42.

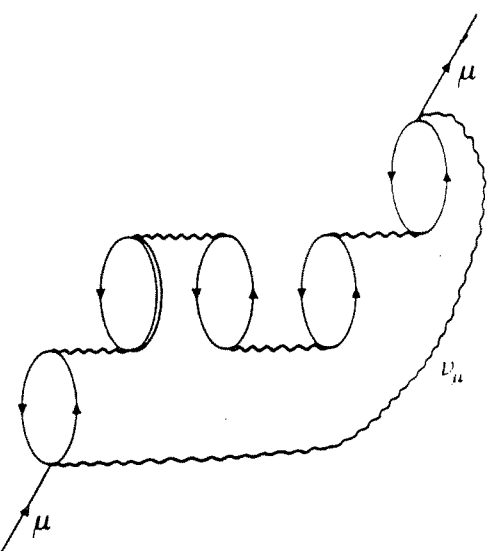

Fig. 13. Many-body Feynman diagrams accounting for the medium polarization in the spin-isospin channel driven by the $\mu^- \mathrm{p} \rightarrow \mathrm{n}\nu_\mu$ transition.

The sum implicit in Fig. 13 leads to two independent geometric series in the longitudinal and transverse channels (the term with g_{A}^2 involves the trace of $g_{\mathrm{A}}^2 \sigma_i \sigma_i \bar{U}$,

which can be equivalently written as $g_A^2 \sigma_i \sigma_j \bar{U}[\hat{q}_i \hat{q}_j + (\delta_{ij} - \hat{q}_i \hat{q}_j)]$, explicitly separated into a longitudinal and a transverse part). After a little of algebra one finds that the renormalization can be taken into account by substituting

$$g_A^2 \mathrm{Im}\,\bar{U} \rightarrow g_A^2 \left(\frac{1}{3} \frac{\mathrm{Im}\,\bar{U}}{|1 - U V_l|^2} + \frac{2}{3} \frac{\mathrm{Im}\,\bar{U}}{|1 - U V_t|^2} \right), \tag{50}$$

where $U (= U_N + U_\Delta)$ is the Lindhard function defined in Eq. 24 which accounts for p-h as well as Δ-h excitations in Fig. 13. In obtaining Eq. 50 above, the fact that U_Δ does not have an imaginary part, in the kinematical regime explored by the muon capture process, has been taken into account.

The pieces involving the pseudoscalar term, g_P, behave differently. Indeed the $g_P \vec{\sigma} \vec{q}$ coupling, in the non-relativistic limit, singles out the longitudinal part of the interaction and the renormalization is then

$$g_P^2 \,\mathrm{Im}\,\bar{U} \rightarrow g_P^2 \frac{\mathrm{Im}\,\bar{U}}{|1 - U V_l|^2}\,. \tag{51}$$

Analogously, the terms involving g_M single out the transverse part of the interaction and we have

$$g_M^2 \,\mathrm{Im}\,\bar{U} \rightarrow g_M^2 \frac{\mathrm{Im}\,\bar{U}}{|1 - U V_t|^2}\,. \tag{52}$$

The other terms, which are rather small, are not renormalized.

After performing the renormalization of Eq. 48, we obtain the new capture width $\hat{\Gamma}(\rho_p, \rho_n)$. The local density approximation (LDA) to go to finite nuclei is obtained by replacing $\rho_p \rightarrow \rho_p(r)$, $\rho_n \rightarrow \rho_n(r)$ for the actual nuclei and evaluating

$$\Gamma = \int \mathrm{d}^3 r |\Phi_{1s}(\vec{r})|^2 \hat{\Gamma}(\rho_p(r), \rho_n(r))\,, \tag{53}$$

where $\Phi_{1s}(\vec{r})$ is the muon wave function in the 1s state from where the capture takes place. The LDA assumes implicitly a zero range of the interaction, or no dependence on $\vec{q}$ equivalently. The q-dependence of the form factors is extremely weak and thus the LDA prescription becomes highly accurate [16].

Note that the approach of reference [16] and presented here differs substantially from standard ones, which require the evaluation of two-body matrix elements for the ground state of the nucleus. In this approach, one does not evaluate any nuclear matrix element and the only nuclear information needed is the proton and neutron densities. As pointed out in the introduction some approaches use a closure sum over the nuclear intermediate states [17–19]. Others, more elaborated and accurate [20], use a sum rule approach which still relies upon an average excitation energy, although the dependence of Γ on this variable is rather smooth, unlike in the closure sum case. Here the Lindhard function has summed the contribution from intermediate nuclear states (the excited states of neutrons on top of the Fermi sea). On the other hand, the concept of Z_{eff} has not been needed. Equation 53 provides Γ directly from the muon wave function and the function $\hat{\Gamma}(\rho_p(r), \rho_n(r))$.

3.3 Results

A rather exhaustive list of nuclei was studied in Ref. 16. In this reference results for nuclei from ^{6}Li ($\Gamma \approx 0.3 \times 10^4 s^{-1}$) up to ^{209}Bi ($\Gamma \approx 0.15 \times 10^8 s^{-1}$) are presented. The overall agreement between the theoretical results and the experiment is spectacular considering the amount of nuclei studied and the large variation of the rates (four orders of magnitude) from light to heavy nuclei. In Fig. 14, a selection of the most stable isotopes as a function of Z are shown in order to give a visual idea of the quality of the agreement found in Ref. 16.

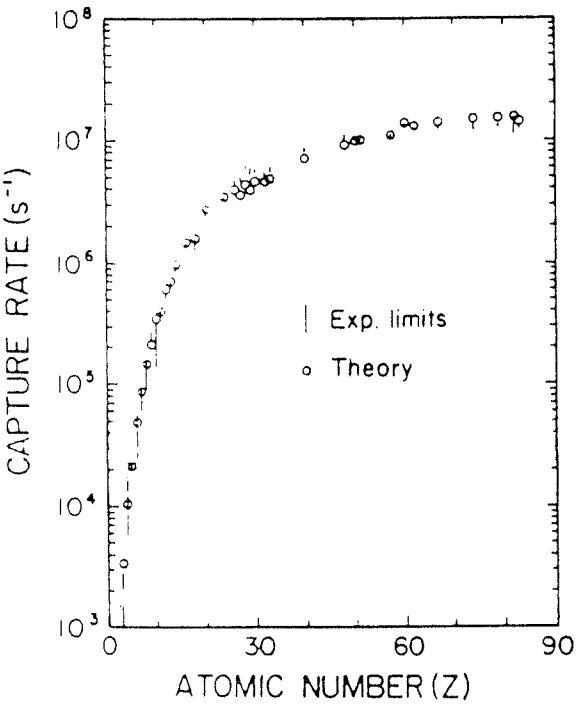

Fig. 14. Total rates for negative muons captured by the most stable isotopes from [16]. Circles are theoretical results. Experimental limits from different groups are also shown.

In Ref. 16, the effects of the muon momentum and binding energy, Pauli blocking (which turns out to be very important, because the outgoing n in the $\mu^- p \rightarrow n\nu_\mu$ reaction can not go to any of the neutron occupied states[10])) on the rate are carefully examined. Here, we will concentrate on the effects of the renormalization discussed briefly in section 3.2 and more carefully in Ref. 16. These effects play a very important role in this problem. Indeed, in Fig. 15 the results calculated with and without the renormalization as a function of Z are shown. For medium and heavy nuclei the nuclear renormalization reduces the results by about a factor two and it is essential to produce agreement with the experimental numbers. This is a very interesting process, which evidences the strong nuclear renormalization on top of the weak interaction process, which can be brought under control as we have shown here. Although similar effects due to the spin-isospin polarization of

[10]) This is taken into account by means of the factor $1 - n_2(k)$ in the Lindhard function of Eq. 49.

the nucleus also appear in many nuclear processes, sometimes it is more difficult to asses their importance since the nuclear interaction itself can be less controllable. However, it is interesting to mention that these medium polarization effects have been also considered (as we will see during these lectures) in connection with the problem of Σ-atoms and hypernuclei, Λ hypernuclei, K^+-nucleus scattering, pionic atoms, π-nucleus scattering at low energies ... The clean effects of this medium renormalization shown here stress and reinforce the interpretation given for these other phenomena.

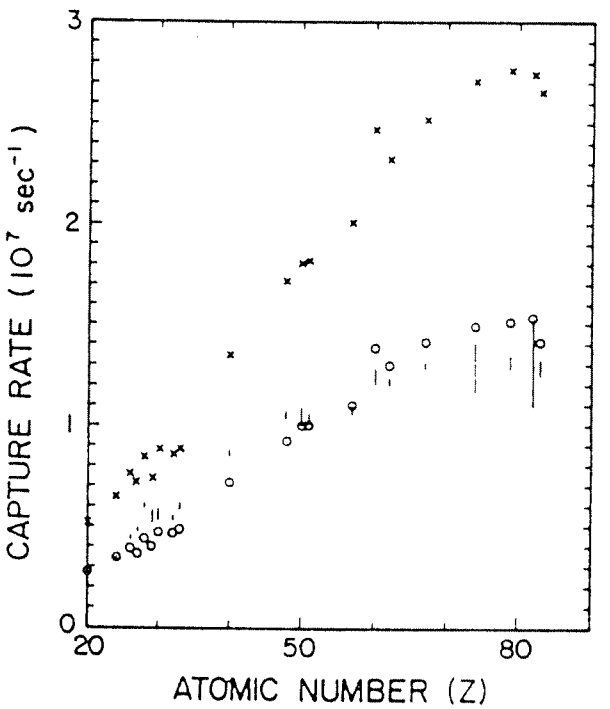

Fig. 15. The nuclear medium renormalization effect in the calculation of the total nuclear capture rates of μ^- from [16]. Crosses and circles are calculation without and with the renormalization respectively.

4 Σ hypernuclei and atoms[11])

The case of the Σ^- atoms and Σ hypernuclei offers a very interesting example of the density effects in the Σ-nucleus interaction. The hyperon Σ in a nucleus can decay strongly through the channel $\Sigma N \to \Lambda N$. This reaction does not violate strangeness and hence proceeds via strong interaction.

In the case of the Σ^- hyperon, the Coulomb potential alone, irrespective of the strength of the short-range nuclear potential, is enough to bind Σ^- atomic states. Some of these states (the most bound) are such that the Σ-wavefunction is essentially inside of the nucleus, hence the name hypernuclei is more suited to them, although there is a gradual transition from these hypernuclear states to more

[11]) This section is based on Ref. 21.

properly called Σ^- atoms [22], where the orbits are far away from the nucleus. The question of the observability of Σ-hypernuclear states depends upon their width and the energy separation between the levels. If the width is larger than the level separation such hypernuclear states will not be observed in any nuclear reaction (the most used have been of the type (K^-, π) [23, 24] and (π, K^+) first proposed in [25]). Although many Σ^- atomic states are known [22] there is a limitation to the observability of such states given by the detection method. The Σ^- (as in the case of π^- atoms) cascades down through atomic orbits and approaches to the nucleus. The absorptive width increases in this process and when it exceeds the radiative width, the Σ particle gets absorbed by the nucleus and no further level of smaller energy can be reached. However, such states exist and their observation would be most interesting to get a proper understanding of the dynamics of the Σ-nucleus interaction. No such states have been clearly observed yet. On the other hand there is the possibility that there are bound states of Σ^0 or Σ^+ hypernuclei.

The experimental situation is very unclear, ten years ago there were some claims at CERN [23] of sharp peaks in the (K^-, π) which would correspond to Σ-hypernuclear states in ^{12}C and ^{16}O with widths of around 5 MeV and most recently at KEK there were signals of a possible bound state of the $^4_\Sigma$He hypernucleus[12]) in the (K^-, π^+) reaction [24]. In both cases, new experiments designed to confirm these findings failed to do it[13]) and one of the few evident conclusions is that more statistics and more experiments are needed to clarify the situation.

In spite of the limited experimental information available, the possible discovery of the sharp resonances stimulated much theoretical work aiming at understanding the origin of such narrow widths, since simple estimates provide widths between 20–30 MeV for the Σ-hypernuclear states[14]). This is compatible with empirical determinations of the Σ^--nucleus optical potential, from Σ^--atoms data (energy shifts and widths) [22]

$$\begin{aligned} V(r) &= -U(r) - \mathrm{i}W(r)\,, \\ U(r) &= (28 \pm 3)\frac{\rho(r)}{\rho_0} \quad [\mathrm{MeV}]\,, \\ W(r) &= (15 \pm 2)\frac{\rho(r)}{\rho_0} \quad [\mathrm{MeV}]\,. \end{aligned} \tag{54}$$

We see that through $\Gamma \approx 2\,W$ for $\rho = \rho_0$, one obtains $\Gamma \approx 30$ MeV, as the estimate based on the cross section gives. Solving numerically the Schrödinger equation with the potential of Eq. 54 one gets widths with values around of 20 MeV.

In the rest of this section, we will present an approach [21] to the problem based on the use of the induced interaction, discussed in section 2.2, which provides small widths for the bound hypernuclear states, being at the same type compatible with

[12]) With a binding energy of about 3.2 MeV and a width of 4.6 MeV.

[13]) See for instance the discussion in [21].

[14]) A simple estimate of the hypernuclear width through the formula $\Gamma \approx \sigma\rho v_{\mathrm{rel}}$, with σ the cross section for the $\Sigma N \to \Lambda N$ reaction and v_{rel} the relative velocity of the ΣN system, gives $\Gamma \approx 30$ MeV for $\rho = \rho_o$.

the Σ^--atom data. The Σ^- atomic information is re-analyzed from this point of view and its information is used to obtain energies and widths of more bound $\Sigma^{-,0,+}$ states of the hypernuclear type. One obtains in this way many bound states in light and medium nuclei, where the widths are narrower than the separation between the levels.

4.1 Quenching of the imaginary part of the Σ-nucleus optical potential

We should note that the density regimes of the Σ^- atoms and Σ hypernuclei are very different. While in the Σ^- atomic states, the Σ^- has little overlap with the nucleus, feeling effective densities around $\rho = 0.1\rho_0$, in the Σ hypernuclei the Σ will feel nuclear densities of the order of ρ_0. This is a place where a density dependence in the imaginary part of the self-energy would manifest itself clearly, given the two very distinct density regimes where the atoms or the hypernuclei live.

We can construct the Σ self-energy piece containing the $\Sigma N \to \Lambda N$ transition. This is depicted in Fig. 16 as a standard many-body diagram. We shall call Σ^* the Σ self-energy inside of the nuclear medium, equivalent to the optical potential.

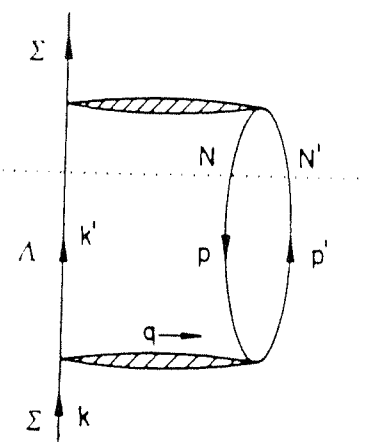

Fig. 16. Many-body Feynman diagram for the Σ self-energy incorporating the $\Sigma N \to \Lambda N$ transition. The dotted line indicates the cut leading to $\mathrm{Im}\,\Sigma^*$ when the particles cut by this line are placed on-shell in the integration over the internal variables.

The Σ has isospin $T = 1$ and the Λ, $T = 0$. This forces the exchanged objects responsible for the interaction $\Sigma N \to \Lambda N$ to carry $T = 1$, Fig. 17. There is a possibility of having $\Sigma N \to \Lambda N$ mediated by kaon exchange but this contribution is rather small [26]. Hence we are left with the spin-isospin channel, about which we are turning around these lectures. We can again use the $\pi + \rho$ model modified by short range correlations as we did in Eq. 40. Only the couplings and the short distance correlations are now different. The new couplings are given by ([27])

$$\frac{f^2_{\Sigma\Lambda\pi}}{4\pi} = 0.019\,,$$

$$\frac{f^2_{\Sigma\Lambda\rho}}{4\pi} = 2.30\,. \tag{55}$$

As it was discussed for the case of the NN interaction in section 2.2, the short-range repulsive potential part can be very well approximated by means of a local correlation function. The $\Sigma N \rightarrow \Lambda N$ effective interaction (G-matrix) in a good approximation is

$$G_{\Sigma N\rightarrow\Lambda N}(r) = g(r)V_{\Sigma N\rightarrow\Lambda N}\,, \tag{56}$$

given by [21] where $V_{\Sigma N\rightarrow\Lambda N}$ represents the potential due to $\pi + \rho$ exchange and with $g(r)$ a typical correlation function which vanishes as $r \rightarrow 0$ and goes to 1 as $r \rightarrow \infty$. This procedure is quite appropriate to the present case because it allows us to include the effect of the hard core used in the $\Sigma N \rightarrow \Lambda N$ transition potential in the analysis of [27]. We shall use a practical correlation function

$$g(r) = 1 - j_0(q_c r) \tag{57}$$

by means of which we obtained a fair reproduction of a realistic correlation function in the NN interaction with values $q_c \approx 780\,\mathrm{MeV}/c$. The value of q_c should not necessarily be the same here given the different nature of the forces. In this case q_c should be indicative of the inverse of the hard core radius r_c of the analysis of [27], $q_c \approx 500\,\mathrm{MeV}/c$.

Hence we get now different longitudinal and transverse effective interactions: V_l^Σ, V_t^Σ, which can be obtained from the expressions of Eq. 41 by using the new value of q_c and replacing $f_{\pi NN}$ and $f_{\rho NN}$ by $f_{\Sigma\Lambda\pi}$ and $f_{\Sigma\Lambda\rho}$ given in Eq. 55.

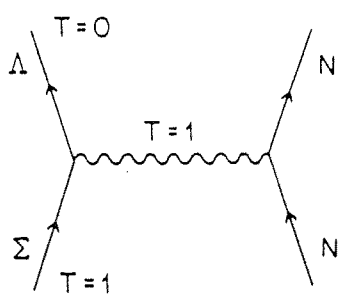

Fig. 17. The $\Sigma N \rightarrow \Lambda N$ interaction mediated by an object of isospin $T = 1$ in the t-channel.

We have carried out the first part of the program in constructing the induced interaction. So far we have constructed the transition G-matrix or effective interaction. The next step is to take into account the p-h and Δ-h excitations to all orders in the RPA sense produced by the spin-isospin $\Sigma N \rightarrow \Lambda N$ interaction. This is depicted diagramatically in Fig. 18 for the particular case that we have here. Note that the first p-h or Δ-h excitation is produced by $G_{\Sigma N\rightarrow\Lambda N}$, but after that, all the new excitations are produced by the NN or NΔ effective interactions. Since the interaction responsible for the $\Sigma N \rightarrow \Lambda N$ transition carries $T = 1$ in the spin

channel, as we discussed above, this will automatically select the spin-isospin channel of the NN or NΔ effective interactions between the p-h or Δ-h for which we use the expression of Eq. 40, and equivalent expressions for the NN $\to$ NΔ transition or NΔ $\to$ NΔ interaction by changing $\vec{\sigma} \to \vec{S}$, $\vec{\tau} \to \vec{T}$ and f by f^* for each Δ involved.

The other ingredient needed to construct the induced interaction is the polarization contribution provided by the p-h or Δ-h excitation. This is done by means of the Lindhard functions $U_{\rm N}$ and U_Δ defined in Eqs. 16 and 25.

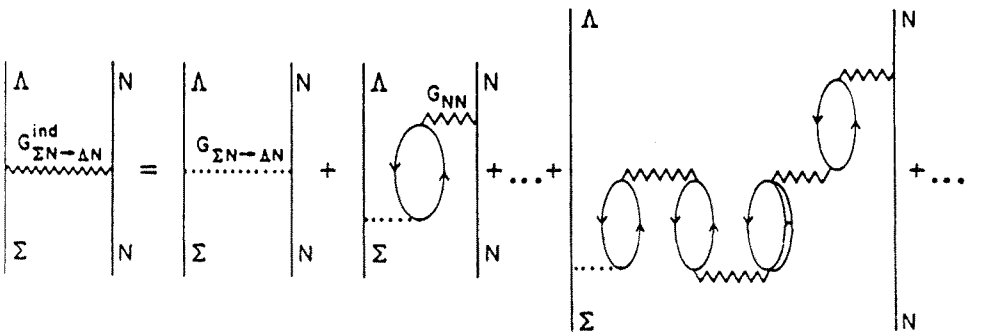

Fig. 18. RPA series for the induced ΣN $\to$ ΛN interaction of Eq. 58. Both p-h and Δ-h excitations ($U_{\rm N,\Delta}(q)$) are included, as well as the p-h and Δ-h interaction ($V_{\rm l,t}(q)$ in $G_{\rm NN}$) between them. $G_{\Sigma{\rm N}\to\Lambda{\rm N}}$ is the effective interaction.

With the splitting of the interaction into longitudinal and transverse parts the sum implicit in Fig. 18 can be easily done and it amounts to summing two independent geometrical series, one for the longitudinal part and another one for the transverse part, as in Eq. 43. One finds

$$G^{\rm ind} = \left[\frac{V_{\rm l\Sigma}(q)}{1-U(q)V_{\rm l}(q)}\hat{q}_i\hat{q}_j + \frac{V_{\rm t\Sigma}(q)}{1-U(q)V_{\rm t}(q)}(\delta_{ij}-\hat{q}_i\hat{q}_j)\right]\sigma_i^{(1)}\sigma_j^{(2)}, \qquad (58)$$

with $U(q)$ defined in Eq. 24.

Now, we are in disposition of calculating the Σ self-energy, Σ^*, due to the ΣN $\to$ ΛN transition inside of the nuclear medium (Fig. 16). By following the standard Feynman rules [1, 2] one finds

$$-{\rm i}\Sigma^*(k) = -\int\frac{{\rm d}^4p}{(2\pi)^4}\int\frac{{\rm d}^4q}{(2\pi)^4}\frac{{\rm i}\,n(\vec{p})}{p^0-E_{\rm N}(\vec{p})-{\rm i}\epsilon}\frac{{\rm i}\,(1-n(\vec{q}+\vec{p}))}{q^0+p^0-E_{\rm N}(\vec{q}+\vec{p})+{\rm i}\epsilon}$$
$$\times\frac{\rm i}{k^0-q^0-E_\Lambda(\vec{k}-\vec{q})+{\rm i}\epsilon}\sum_{s_{\rm N},s_{\rm N'},t_{\rm N},t_{\rm N'}}\sum_{s_\Lambda}(-{\rm i}T)(-{\rm i}T), \qquad (59)$$

T is the transition amplitude in the ΣN $\to$ ΛN process and s, t stand for the spin and isospin of the internal variables. The self-energy will be independent of the spin and isospin of the Σ in spin saturated symmetric nuclear matter. We can then substitute the sum over spins and isospins of T^2 by $2\overline{\sum}\sum T^2$, where now we sum over spins of Λ, N (final state), and average over spins of Σ, N (final state). In the

model presented here [21] $2\overline{\sum}\sum T^2$ depends only on the momentum transfer. This allow us to carry out the integral over $\vec{p}$ since only the particle-hole propagator depends on it. By recalling Eqs. 16 and 9 for the Lindhard function we identify this integral with the first term of Eq. 9. However, the Lindhard function contains an additional term (second term of Eq. 9). By including this term we are adding the left diagram of Fig. 19 to the right one of the same figure, already considered for the Σ self-energy. This additional diagram only contributes to the real part of Σ^*. Thus we can now write

$$\Sigma^*(k) = \frac{\mathrm{i}}{2}\int \frac{\mathrm{d}^4q}{(2\pi)^4} U_{\mathrm{N}}(q) \frac{\overline{\sum}\sum T^2}{k^0 - q^0 - E_\Lambda(\vec{k}-\vec{q}) + \mathrm{i}\epsilon}\,. \tag{60}$$

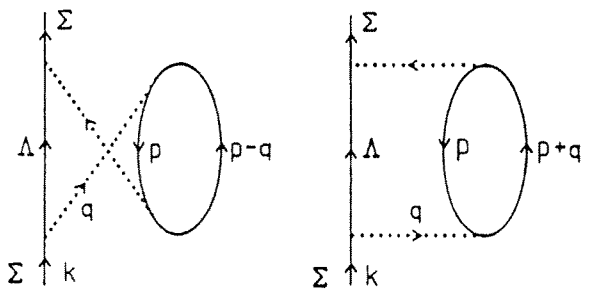

Fig. 19. Σ self-energy diagrams included in Eq. 60. Right: Direct graph contributing to both Re Σ^* and Im Σ^*. Left: New graph contributing to Re Σ^* only.

The T-matrix contain terms like $((q^0)^2 - \vec{q}^{\,2} - m_i^2 + \mathrm{i}\eta)^{-1}$, hence the poles of T lie in the second and fourth quadrant of the complex q^0 plane, as shown in Fig. 20. As it was discussed in Fig. 6 the Lindhard function $U(q)$ has cuts also in the second and fourth quadrant of the complex q^0 plane. The remaining analytical structure in the complex q^0 variable can been seen in Fig. 20. This particular structure suggests a Wick rotation to perform the q^0 integration. Thus

$$\int_{-\infty}^{+\infty} \mathrm{d}q^0 + \int_C \mathrm{d}q^0 + \int_{+\mathrm{i}\infty}^{-\mathrm{i}\infty} \mathrm{d}q^0 = 2\pi\mathrm{i}\,\mathrm{Res}(q^0 = k^0 - E_\Lambda) \times \theta(k^0 - E_\Lambda(\vec{k}-\vec{q}))\,, \tag{61}$$

where C stands for the circles in the infinity in Fig. 20. Since the integral over C vanishes one finds (note that T^2 is a real function which depends on q^0)

$$\Sigma^*(k) = \mathrm{i}\int \frac{\mathrm{d}^3q}{(2\pi)^3}\int_{-\mathrm{i}\infty}^{+\mathrm{i}\infty} \frac{\mathrm{d}q^0}{2\pi}\,\frac{U_{\mathrm{N}}(q)}{2}\,\frac{\overline{\sum}\sum|T|^2}{k^0 - q^0 - E_\Lambda(\vec{k}-\vec{q})} + \int \frac{\mathrm{d}^3q}{(2\pi)^3}\,\frac{U_{\mathrm{N}}(q)}{2}\theta(q^0)\overline{\sum}\sum|T^2|_{q^0=k^0-E_\Lambda(\vec{k}-\vec{q})}\,, \tag{62}$$

where the first term provides only a real background, while the second gives rise to both a real and an imaginary part.

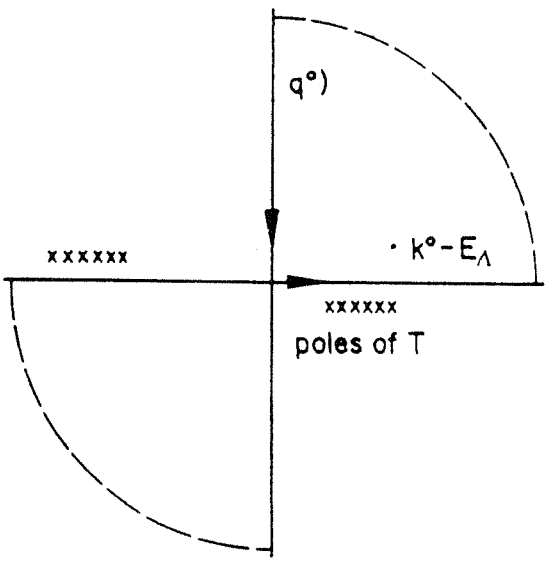

Fig. 20. Analytical structure of the integrand of Eq. 60 in the complex variable q^0. Shown in the figure is the Wick rotation used to perform the integration over q^0.

Inclusion of the induced interaction leads from Fig. 19 to Fig. 21 and results in the substitution in Eq. 62 of

$$U_{\rm N}\,\overline{\sum}\sum|T|^2 \equiv U_{\rm N}(q)\left(V_{\rm l\Sigma}^2(q)+2V_{\rm t\Sigma}^2(q)\right)$$
$$\rightarrow \frac{U(q)V_{\rm l\Sigma}^2(q)}{1-U(q)V_{\rm l}(q)}+\frac{2U(q)V_{\rm t\Sigma}^2(q)}{1-U(q)V_{\rm t}(q)}\,. \qquad (63)$$

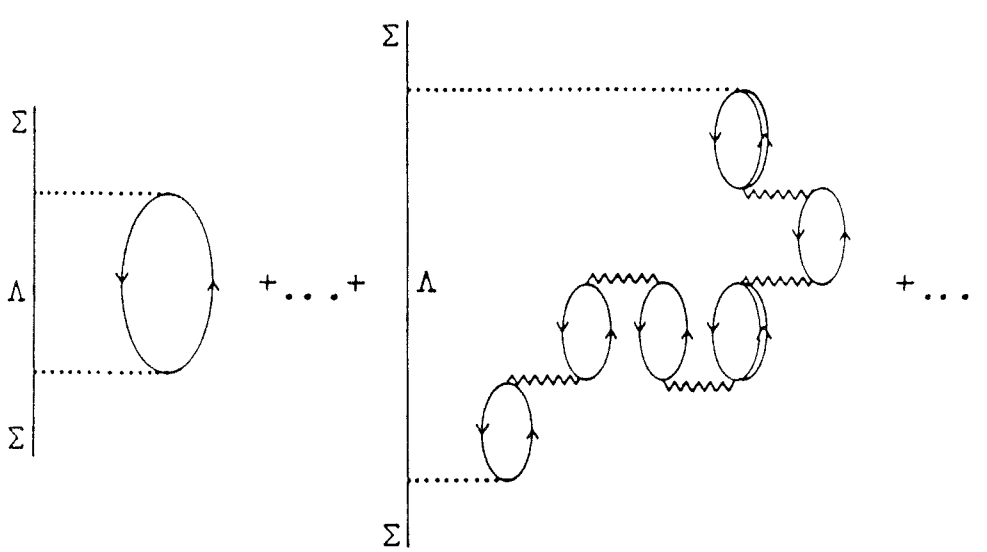

Fig. 21. Diagrams contributing to the Σ self-energy, once the induced interaction is included.

The final expression for the Σ self-energy is then obtained from Eqs. 62 and 63. In particular for its imaginary part, taking into account that $V_{l,t}$ and $V_{l,t}^{\Sigma}$ are real, one finds

$$\mathrm{Im}\,\Sigma^*(k) = \frac{1}{2}\int \frac{\mathrm{d}^3q}{(2\pi)^3}\theta\left[k^0 - E_\Lambda(\vec{k}-\vec{q})\right] \left[\frac{\mathrm{Im}\,U(q)V_{l\Sigma}^2(q)}{|1-U(q)V_l(q)|^2} + \frac{2\,\mathrm{Im}\,U(q)V_{t\Sigma}^2(q)}{|1-U(q)V_t(q)|^2}\right]_{q^0=k^0-E_\Lambda(\vec{k}-\vec{q})} . \quad (64)$$

As we discuss at the end of section 2.2 the induced interaction produces an enhancement and a quenching of the longitudinal and transverse modes of the interaction, respectively. The net effect on the quantity $V_{l\Sigma}^2 + 2V_{t\Sigma}^2$ depends on the weight of the longitudinal and transverse parts in this expression. The longitudinal part $V_{l\Sigma}^2$ gives only 8% of the total $V_{l\Sigma}^2 + 2V_{t\Sigma}^2$, while 92% of the contribution in that sum comes from the transverse part $2V_{t\Sigma}^2$ [21]. It is clear after this exposition that the net effect of the induced interaction will be to produce a quenching in the imaginary part of the optical potential Σ-nucleus ($\mathrm{Im}\,\Sigma^*$) as a function of ρ. Coming back to our discussion at the beginning of this section, Σ^- atoms and Σ hypernuclei are then going to feel a very different potential: while for the first ones the effect of the induced interaction will be negligible, for the latter ones this effect is going to play an important role.

In Fig. 22 we show results (from Ref. 26) for $\mathrm{Re}\,\Sigma^*$ and $\Gamma = -2\,\mathrm{Im}\,\Sigma^*$ as a function of the density in lowest order and with the induced interaction. At lowest order (Eq. 62), we can see that the real part is in a good approximation a linear function of the density while the imaginary part shows some quenching at high densities due to the Pauli exclusion principle. The use of the induced interaction (Eq. 63) has a little effect on the real part, however it produces a drastic reduction of $\mathrm{Im}\,\Sigma^*$ at large densities. While at low densities, $\rho \approx 0.1\rho_0$, $\mathrm{Im}\,\Sigma^*(\rho)$ is approximately linear in ρ, it deviates soon from a linear function and shows saturation properties at $\rho \approx 0.6\rho_0$ as a function of the density. One may wonder why one does not find the same quenching in the real part. The reason is that in $\mathrm{Re}\,\Sigma^*$ the range of $\vec{q}$ in the integration is not limited as in $\mathrm{Im}\,\Sigma^*$. Larger values of $|\vec{q}|$ contribute now to the integral and with $U(q) \approx |\vec{q}|^{-1}$ the effects of the renormalization of Eq. 63 are smaller.

4.2 Results

A potential like the one in Fig. 22 leads immediately to narrow hypernuclear states, as it was first pointed out in Reference [26][15]).

At the same time we can see that for low densities, a linear extrapolation of $\Gamma(\rho) = -2\,\mathrm{Im}\,\Sigma^*(\rho)$ from Fig. 22 gives $\Gamma^{\mathrm{ext}}(\rho) \approx 24\rho/\rho_0$ [MeV], which should be compared with $2W(r)$ of Eq. 54 from a best fit to Σ^- atoms data. The theoretical

[15]) In this reference widths of around 5 MeV were found for the 1s and 2p hypernuclear states in ^{12}C and ^{16}O.

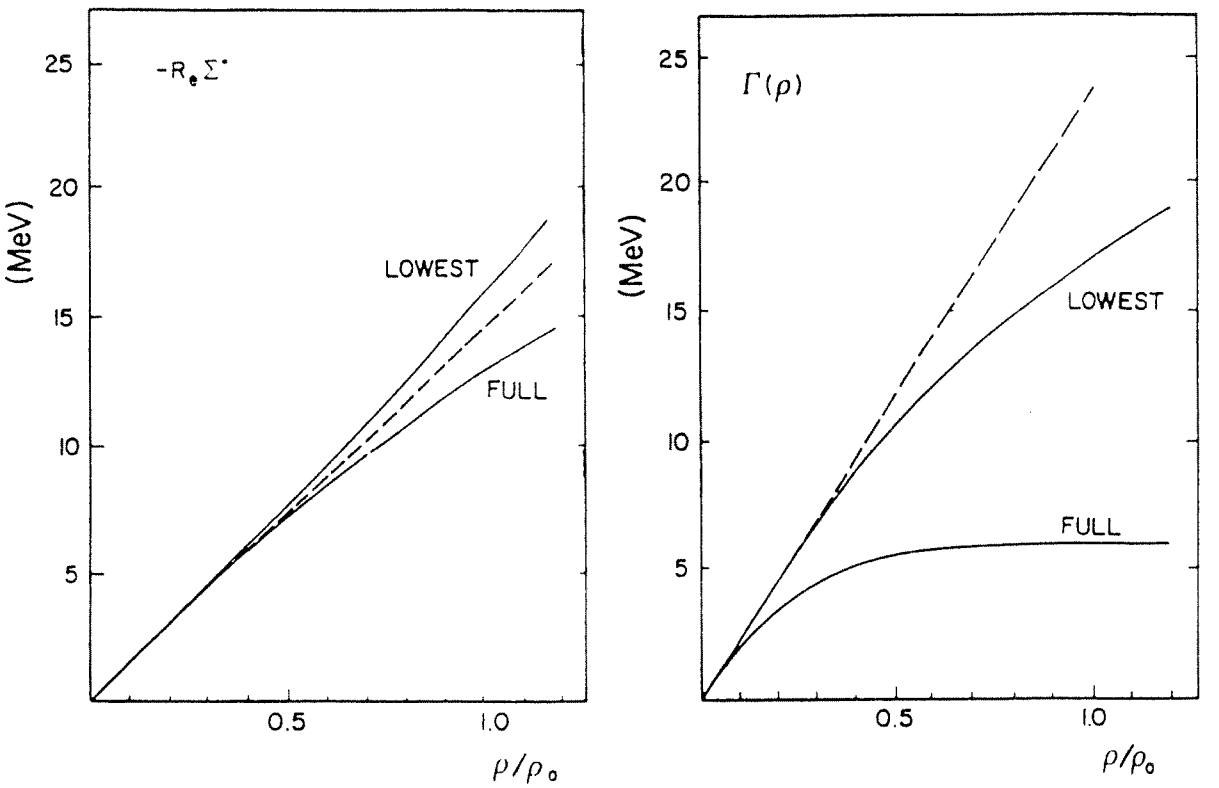

Fig. 22. Results for the Σ self-energy from [26]. Straight line: linear extrapolation from $\rho = 0$. Line labeled as "lowest": lowest order result from Eq. 62. Line labeled as "full": full induced interaction results from Eqs. 62 and 63.

results are about 15 % below those quoted there. This tell us that with that potential, one can now get narrow widths for hypernuclear states and still be consistent with the Σ^- atomic data [28].

The results of Fig. 22 led us to the conclusion that the Σ optical potential has a real part approximately proportional to the nuclear density while the imaginary part has some saturation properties as a function of the density. However, while the evaluation of the imaginary part of Σ^* is rather reliable, the real part presented here, and first evaluated in [26], is only a piece of the total real part of Σ^*, which would also come from other sources, mostly from Hartree pieces. However the results of [26] have the virtue of showing that $\mathrm{Re}\,\Sigma^*$ is in any case approximately linear in the density and so would be the Hartree pieces. Due to this, a parametrization of $\mathrm{Re}\,\Sigma^*$ proportional to ρ seems most indicated.

In order to perform a systematic study of bound states with the Σ nuclear potential one needs the strength of the real part. In Ref. 21 a fit of the optical potential Σ-nucleus to the Σ^- atoms data was done. The real part was taken to be linear in density, whereas for the imaginary part was taken a functional which implemented the saturation properties discussed in Fig. 22. Thus, the following optical potential was used:

$$V(r) = -U(r) - \mathrm{i}W(r)\,,$$

$$U(r) = U_0 \frac{\rho(r)}{\rho_0} \quad [\mathrm{MeV}],$$
$$W(r) = \frac{W_0}{5.2} \arctan\left(\frac{5.2\,\rho(r)}{\rho_0}\right) \quad [\mathrm{MeV}]. \tag{65}$$

The density dependence of $W(r)$ in Eq. 65 is inspired by the results found in Fig. 22. Actually a good fit to $\Gamma(\rho)$ in Fig. 22 can be obtained with values of W_0 of around 12 in Eq. 65. From the fit[16]) to the Σ^- data one gets [21],

$$U_0 = 31 \pm 4 \text{ MeV},$$
$$W_0 = 15 \pm 2 \text{ MeV}. \tag{66}$$

These results are in agreement[17]) with those of the best fit by Batty et al. and quoted above in Eq. 54.

The results obtained in Ref. [21] using the potential of Eq. 65 for Σ^- atoms are quite similar to those obtained with the linear potential of Batty et al. (Eq. 54) and both of them give a fair reproduction of the experimental data. However, for more strongly bound Σ^- states the difference in the shifts and specially in the widths become more apparent, particularly in the hypernuclear states as shown in Table 1.

Table 1. Binding energies (B) and widths (from Ref. 21) of different $\Sigma^{-,0,+}$ hypernuclear states in ^{27}Al and ^{32}S calculated with linear (Eq. 54) and saturating potentials (Eq. 65). All numbers are in keV.

			Σ^-			Σ^0		Σ^+	
			2s	2p	1s	2p	1s	2p	1s
^{27}Al	B	LIN	1148	13800	27208	7256	20152	795	13128
		SAT	3674	14700	27636	8372	20649	2149	13715
	Γ	LIN	10700	23310	28895	22562	28517	21697	28087
		SAT	3580	7060	7683	6894	7638	6655	7581
^{32}S	B	LIN	3622	16040	27581	8549	19514	1113	11493
		SAT	5551	16740	27896	9410	19897	2196	11969
	Γ	LIN	13100	22700	26857	21985	26476	21133	26028
		SAT	4560	7140	7628	6982	7579	6754	7513

In this table (elaborated from the results of Ref. 21) we show energies and widths of the Σ^- hypernuclear states in ^{27}Al and ^{32}S with both potentials[18]). In this table we also show results for $\Sigma^{+,0}$ hypernuclear states, obtained using the same strong potential but killing or making repulsive the Coulomb interaction.

[16]) Solving numerically the Schörodinger equation for the different nuclei with the Coulomb attractive potential in addition to the potential of Eq. 65.

[17]) Note that for low densities, as in the case of Σ^- data, $W(r) \approx W_0 \rho(r)/\rho_0$

[18]) For the linear potential (potential of Batty et al.), a value of 31 MeV for the real part, instead of the value 28 ± 3 MeV quoted in Eq. 54, is used. The reason for this change is that a better fit to the Σ^- atom data is obtained with this new value than with the originally proposed in Ref. 22.

In the case of Σ^- hypernuclei, with the linear potential one finds 1s and 2p states (in the atomic nomenclature) with binding energies of about 28 MeV and 15 MeV respectively. The interesting thing is to note that the widths are of the same order as the binding energies. Since the widths are larger than the separation energies this would rule out the observation of these states. The results with the saturating potential are rather different. The widths are reduced by about a factor 3 or 4. The widths range now from 4 MeV to 8 MeV for the 2p and 1s states. The binding energies increase a bit with respect to the linear potential because the absorptive part of the potential ($\mathrm{Im}\,\Sigma^*$) acts as a repulsive force and the saturation makes this repulsion less effective. As a consequence one can see now that the widths are smaller by a fair amount than the separation energies, which should make these states observable. Results for $\Sigma^{+,0}$ are qualitatively identical.

To conclude, we have seen how the renormalization of the $\Sigma N \to \Lambda N$ interaction inside of the nuclear medium modifies drastically the features of Σ hypernuclei, allowing in most of the cases for their observability, which otherwise would not be possible.

5 Pion-nucleus interaction

In this section we will study the influence of the nuclear medium corrections in the dynamics of a π-nucleus system at low energies. Our discussion will be based on the findings of the Refs. 29 and 30, where more details can be found by the reader.

5.1 Anomalies in pionic atoms

A pionic atom is an example of a hydrogen-like system, with the electron replaced by a negatively charged pion. The interest in such systems originates in the high precision and selectivity which is typical of atomic spectroscopy.

Negative pions are stopped in matter by purely electromagnetic interactions with electrons and nuclei. The pions are first captured into highly excited molecular orbits, substituting for electrons, which are ejected. The pions de-excite stepwise into more tightly bound orbits by the ejection of Auger electrons and emission of X-rays; they are finally centred on the individual nuclei. When the size of the orbits becomes smaller than that of the innermost electron orbit around the nucleus[19]) the pion finds itself in the presence of the unscreened nuclear Coulomb field. Insofar as nuclear effects can be neglected, the physics is now that of the Bohr atom. The pion is the simplest example of a particle with electromagnetic interactions that obeys the Klein-Gordon equation. In fact, these highlying orbits of pionic atoms provide a quantitative test that the Klein-Gordon equation correctly describes the electromagnetic interactions of a boson.

Our primary interest during these lectures is, however, in the strong pion-nuclear interactions. The pion continues decaying down, due to electromagnetic processes, to inner orbits where it start feeling the effect of its strong interactions with the nucleons of the nucleus. They perturb the spectrum of pionic atoms in low-lying

[19]) Note that $m_\pi/m_e \approx 260$.

orbits. The characteristic deviations from the purely electromagnetic spectrum can be accurately measured; they are a unique selective source of information on the pion-nuclear system in the energy region close to threshold ($\omega \approx m_\pi$).

For those states which can be studied experimentally, the probability of finding the pion inside of the nucleus is small. Because of this small overlap, the effect of the strong pion-nuclear interaction can be treated to leading order as a perturbation (few per cent) of the Coulomb energies. In addition to the shift of the atomic level, there will also be a broadening owing to the pion-nucleus absorption. This complex energy "shift" relative to the spectrum in the absence of strong interaction is denoted by

$$\delta E = \epsilon - \tfrac{1}{2}\mathrm{i}\Gamma\,, \tag{67}$$

where ϵ is the strong interaction shift and Γ the absorption width. The sign of ϵ is defined such that a repulsive shift corresponds to $\epsilon > 0$.

When the pion nuclear pion absorption overwhelms the radiative transition, no more pionic levels (binding energies and widths) can be measured by looking at the X-rays from the electromagnetic decay. Thus, the properties of the 1s states are not known for Z larger than about 14, of 2p states for Z larger than about 35, etc... (for instance, for $Z > 14$ the 2p absorption width is around 2 or 3 orders of magnitude larger than the electromagnetic one due to the X-transition 2p $\rightarrow$ 1s and therefore this electromagnetic transition is very difficult to observe). For heavy nuclei like ^{208}Pb, information is available on the 3d and 4f levels.

The strong interaction shifts and widths have been investigated systematically for a large number of nuclei throughout the periodic table. We have very accurate measurements of boths shifts and widths, with precisions better than 5 %, which range from few eV for the 2p levels in the ^{12}C region up to tens of keV for the 3d levels in the ^{208}Pb region. So we have access to a very valuable and accurate experimental information (it explores four orders of magnitude) about the details of the pion-nucleus interaction.

The first theoretical approaches to the problem were based on the impulse approximation in nuclear matter. To first order in the density ρ, the pion self-energy ($\Pi(\omega_\pi)$, ω_π is the pion energy) in nuclear matter or equivalently the pion-nucleus optical potential ($2\omega_\pi V_{\rm op}(\omega_\pi) = \Pi(\omega_\pi)$) is fully determined by the pion-nucleon T-matrix in the vacuum, $\Pi(\omega_\pi) = T(\omega_\pi)\rho$, [31]. Near pion threshold the pion-nucleon T-matrix can be safely approximated by the s- and p-wave contributions.

This leads to the threshold optical potential in coordinate-space for finite nuclei [32]

$$\begin{aligned} 2\omega_\pi V_{\rm op}(\omega_\pi) \;=\; & -4\pi\left[b_0(\rho_{\rm p}(r)+\rho_{\rm n}(r)) + b_1(\rho_{\rm p}(r)-\rho_{\rm n}(r))\right] \\ & +4\pi\left\{\vec{\nabla}[c_0(\rho_{\rm p}(r)+\rho_{\rm n}(r)) + c_1(\rho_{\rm p}(r)-\rho_{\rm n}(r))]\vec{\nabla}\right\} \end{aligned} \tag{68}$$

with $\rho_{\rm p,n}$ the proton and neutron densities. The parameters b_0 (c_0) and b_1 (c_1) are determined in terms of the isoscalar and isovector s- wave (p-wave) πN scattering length (volume) parameters, respectively. To obtain Eq. 68 a certain method to

translate nuclear matter results to finite nuclei has been used. We will not enter into details here, however we just mention that the local density approximation ($\rho_{p,n} \to \rho_{p,n}(r)$) turns out to be exact for the zero-range s-wave part of the optical potential and that the non-local $\vec{\nabla} \ldots \vec{\nabla}$ structure in the p-wave part of the potential comes from translating $\vec{q}^{\,2}$ in nuclear matter (where only forward propagation is allowed) to $\vec{q}\vec{q}'$ in finite nuclei.

The application of the optical potential of Eq. 68 to pionic atoms requires additional ingredients. In particular the phenomenon of pion absorption is a central feature in pionic atoms and must be included in the model. At pion threshold all parameters $b_{0,1}, c_{0,1}$ are real and thus the potential of Eq. 68 is purely real and cannot account for the absorptive widths of the pionic levels. The pion cannot be absorbed by a single nucleon, it is absorbed predominantly by a pair of nucleons[20]), which suggests the following parametrization of the absorptive contribution to the pion-nucleus optical potential [32]

$$2\omega_\pi V_{\rm op}^{\rm abs} = -4\pi \left[B_0 \rho^2(r) - C_0 \vec{\nabla} \rho^2(r) \vec{\nabla} \right]. \tag{69}$$

Here the complex parameters B_0 and C_0 are related to the underlying pair process, with the s- and p-wave pair absorption given by $\mathrm{Im}\, B_0$ and $\mathrm{Im}\, C_0$ respectively. The real parts $\mathrm{Re}\, B_0$ and $\mathrm{Re}\, C_0$, describe the corresponding dispersive contributions.

Phenomenological descriptions of the accurate data on pionic atoms are generally based on the optical potential of Eqs. 68 and 69 with minor variations[21]). It is common in such an analysis to fix the dominant first-order parameters $b_{0,1}$ and $c_{0,1}$ at their empirical values from πN scattering. The absorptive complex constants B_0 and C_0 are treated as free parameters. These type of potentials gave good fits to experimental data for long time[22]). Then, the experimentalists developed new techniques to measure shifts and widths of new deeper atomic levels (1s up to ^{24}Mg, 3d up to ^{209}Bi). One of the interesting surprises of this new wealth of data is that the traditional and successful Ericson-Ericson potential [32] (Eqs. 68 and 69), or equivalent ones, failed to reproduce the new widths and shifts, and systematic discrepancies remained with some of the data. Particularly the 3d widths of heavy nuclei (Au, Pt, Pb, Bi) and the 1s levels in not so light nuclei (Mg, Al, Si) were grossly overestimated. Serious attempts to solve these "anomalies" have been made by changing the potential, using different parametrizations, but the discrepancies

[20]) At threshold, three or more nucleon pion absorption is much smaller than two nucleon processes.

[21]) In addition to some small kinematical corrections, there is an important and well established ingredient which must be added: the Lorentz-Lorenz correction. It is implemented by the following substitution [32,29] in the p-wave of the pion-nucleus optical potential

$$4\pi \vec{\nabla} f(r) \vec{\nabla} \to 4\pi \vec{\nabla} \frac{f(r)}{1 + 4\pi g' f(r)} \vec{\nabla}, \tag{70}$$

where the Lorentz-Lorenz g' parameter turns out to coincide with the Landau-Migdal parameter introduced in Eq. 44 in the context of NN interaction [29].

[22]) For an excellent review of results obtained with these type of potentials see Ref. 33.

with experiment remained. An excellent review of the so called "anomalies" in pionic atoms can be seen in Ref. 34. Further improved results are obtained with the potential of Ref. 35 where the isospin dependence of the second-order parameter was left free and fitted to the data. The results of this unconstrained fit do not stand a physical interpretation. In physical terms it implies a large amount of π^- absorption by nn pairs, which is forbidden by electric charge conservation, and for some combinations of neutron and proton densities it produces negative probabilities of pion absorption [36].

In what follows, we will present the main features of a microscopical model, devoloped in Refs. 29 and 30, of the pion nucleus optical potential at low energies and at pion threshold. This model provides a density dependent potential where each term has a theoretical ground and a relation to the interaction mechanisms in the system. The essential new ingredients which have been added to the Ericson-Ericson's picture are the use of the RPA induced interaction in a nuclear medium (discussed in Eq. 43) and the explicit calculation of the isospin dependence. These new ingredients lead to a highly non-quadratic density dependence of the imaginary part of the optical potential pion-nucleus, which shows saturating properties as the density increase (as we have seen in the case of Σ hypernuclei and atoms) which provides a reasonable description of the currently known pionic atom data (including the so called "anomalous" data) and pion-nucleus scattering at low energies.

5.2 Pion-nucleus optical potential. Results for pionic atoms

The model for the pion nucleus optical potential contains the mechanisms up to the level of 2p-2h excitations. 3p-3h mechanisms have been shown to be negligible at low energies. The diagrams considered are depicted in Fig. 23.

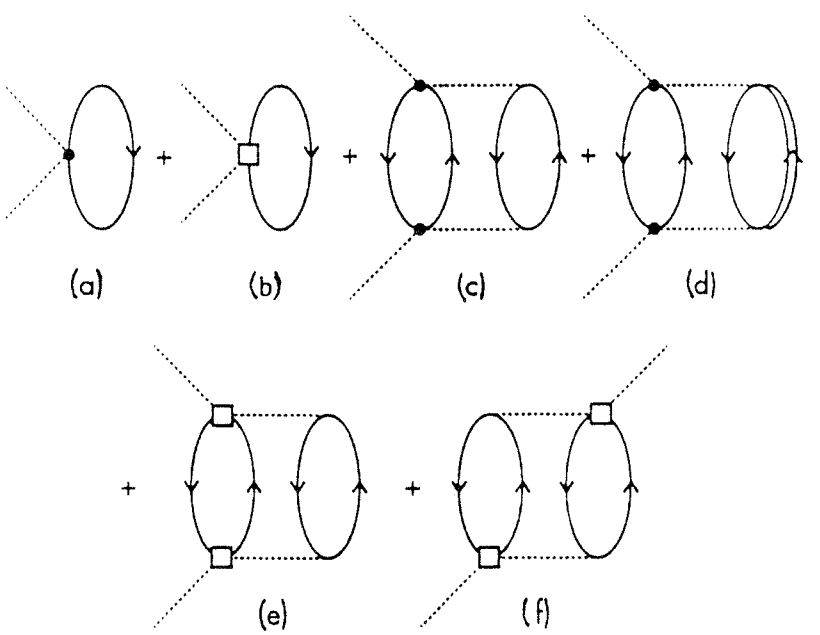

Fig. 23. Diagrams used in the evaluation of the pion nucleus optical potential.

The black dot in Fig. 23 represents the πN s-wave effective interaction, which has been taken from the experimental on shell s-wave T-matrix, and the off-shell extrapolation has been taken from Ref. 37. The white square in Fig. 23 represents the p-wave πN amplitude, which consists of nucleon and delta direct and crossed pole terms of Fig. 9. One of the exchanged pion lines in Fig. 23 is replaced by the full RPA induced interaction where meson exchange and short range correlations are included, Eq. 43. At energies above threshold the imaginary part of the potential associated to quasielastic scattering is included and the second order Pauli corrected rescattering pieces are kept in all cases. The calculations, in Refs. 29 and 30, are carried out in isospin asymmetric nuclear matter and these results are applied to finite nuclei by means of a local density prescription.

The important new features of this potential are:

i) Isospin dependence of the imaginary part of the potential, in particular that of the s-wave. For the s-wave, the structure $(\rho_p + \rho_n)^2$ obtained in symmetric nuclear matter is replaced by $2(\rho_p^2 + \rho_n^2)$ in asymmetric nuclear matter (equally normalized for $N = Z$). For the p-wave, the nuclear pion absorption occurs predominantly on a deuteron-like nucleon pair at short distances. The interaction is then proportional to the product of the average neutron and proton densities $\rho_p(r)\rho_n(r)$, and hence the functional $(\rho_p + \rho_n)^2$ in symmetric nuclear matter should be replaced by $4\rho_p\rho_n$ (again equally normalized for $N = Z$). We will see that the basic problem in the anomalies is an imbalance between the data in light nuclei and in heavy ones. For light nuclei, with $N \approx Z$, all functionals $(\rho_p + \rho_n)^2$, $2(\rho_p^2 + \rho_n^2)$ and $4\rho_p\rho_n$ give the same results. However for heavy nuclei, let us take ^{208}Pb for instance, with respect to a standard $(\rho_p + \rho_n)^2$ potential the $2(\rho_p^2 + \rho_n^2)$ structure of the s-wave reduces the strength of this part by 27%, while the approximate structure $4\rho_p\rho_n$ of the p-wave reduces it by about 5 %. Altogether this means that the 3d width is reduced by about 15 % (assuming equal contribution to the width of both s- and p-waves [29]) with respect to a standard $(\rho_p + \rho_n)^2$ potential.

ii) Density dependence, showing saturating properties as the density increases, of the imaginary part of the p-wave part of the potential[23]). This quenching of the imaginary part of the p-wave potential at high densities is due to the Lorentz-Lorenz effect (Eq. 70) and the polarization of the medium by the spin-isospin interaction, which is the main topic of these lectures.

To understand the origin of this quenching at high densities due to the polarization of the medium, we are going to consider one of the most important contributions to the imaginary part of the pion-nucleus p-wave optical potential. This is depicted in Fig. 24 and corresponds to the contribution of the Δ-h excitation to the imaginary part of the p-wave optical potential. It contributes through the Δ self-energy inside of the nuclear medium. If we look at the most elementary Δ self-energy diagram shown in Fig. 25, we would get an

[23]) Calculations show that the density dependence of the imaginary part of the s-wave potential is in good approximation quadratic [37]. The main reason for that is that in the s-wave only pion exchange (purely longitudinal) is allowed with no short distance correlations or transverse, which is responsible for the quenching, contributions.

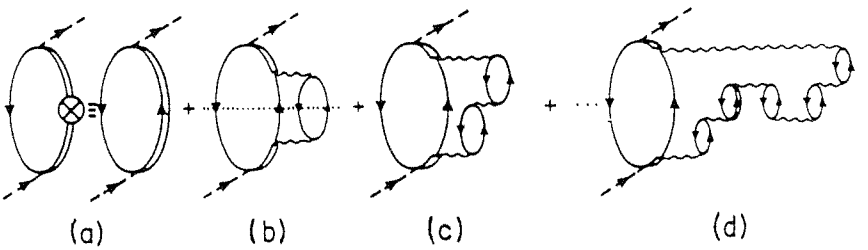

Fig. 24. Feynman diagrams for the direct Δ-h excitation term including Δ self-energy corrections. The diagrams (b)–(d) give rise to an imaginary part of the pion self-energy since they incorporated the pion absorption channels. The dotted line in (b) shows explicitly the intermediate state, 2p-2h, coming from pion absorption. The RPA diagrams in (c) and (d) are responsible for the nonlinear dependence of the Δ self-energy on the nuclear density.

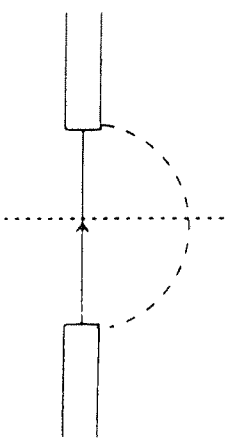

Fig. 25. Δ self-energy diagram.

imaginary part for the Δ self-energy when the lines cut by the dotted line are placed on shell. At pion threshold, this diagram does not contribute to the imaginary part of the pion self-energy, because there is no available phase space. To evaluate the medium corrections to the Δ self-energy of Fig. 25 inside nuclear matter we proceed by renormalizing the N and π propagators. If we dress the pion propagator with one p-h excitation we are left with the diagram of Fig. 26, where one realizes that with a transition from the $T = 3/2$ to the $T = 1/2$ states one needs, as in the case of the Σ self-energy in the previous section, a $T = 1$ object. This can be a pion or rho meson, and according to the arguments of the preceding section and section 2.2, we should use there the effective spin-isospin interaction in a first stage and the induced interaction ultimately (Fig. 27) and obtain in this way the diagrams shown in Fig. 24.

As in the case of Σ hypernuclei, in Ref. 29 an important quenching of the imaginary part of the Δ self-energy was found at high densities, which gets translated in a similar effect on the imaginary part of the p-wave pion-nucleus optical potential.

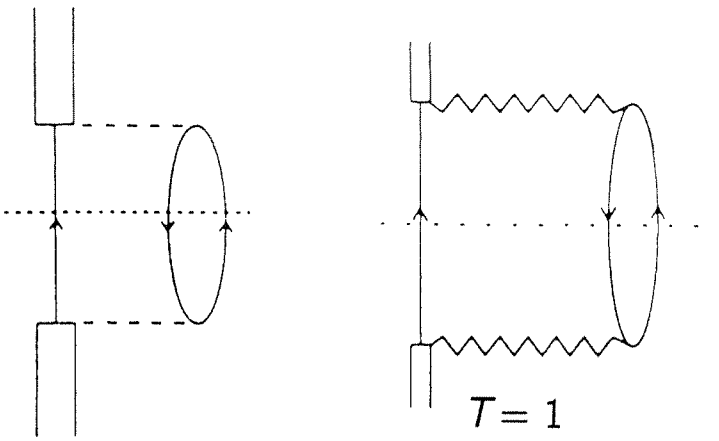

Fig. 26. Δ self-energy diagram in nuclear matter. Left: mediated by pion exchange. Right: mediated by the spin-isospin effective interaction.

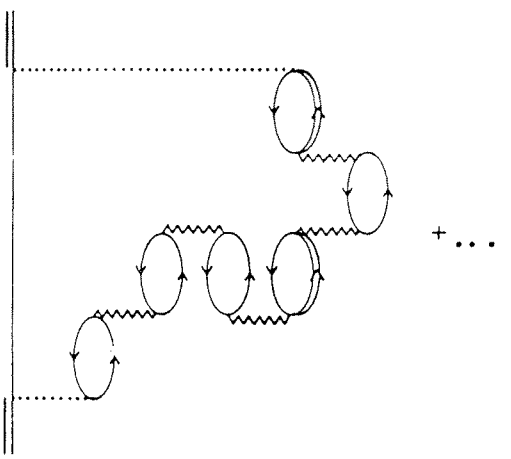

Fig. 27. Δ self-energy diagram through exchange of the spin-isospin induced interaction.

We should now try to understand the effect on shifts and widths of the saturating density dependence of the imaginary part of the pion-nucleus optical potential. The standard potentials which fit the "non anomalous" data feel an effective density [33]. But looking at such different levels as 2p for light nuclei (for instance ^{16}O) and 3d for heavy nuclei, the density felt by those states is quite different, then no longer an effective density is valid. A quenching in density is brought by $\mathrm{Im}\, V^p$ being proportional to $\rho\hat{\rho}$. $\hat{\rho}$ has a saturating behaviour in density as shown in Fig. 28 and this provides a smaller ratio of widths of 3d levels in heavy nuclei (in the region of lead) to widths of 2p levels in very light nuclei (in the region of oxygen) in comparison with potentials with a quadratic behaviour in density for the p-wave imaginary part. This quenching is important in getting a global description to all levels and atoms throughout the periodic table.

With this theoretical potential, a fair description of the widths and shifts of the states through the periodic table including the former anomalous atoms is obtained

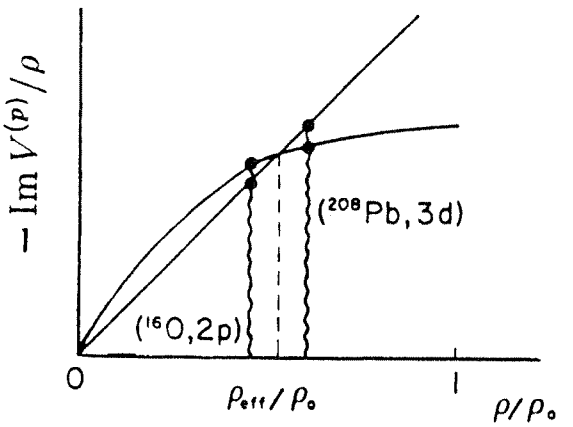

Fig. 28. Typical form of $\mathrm{Im}\,V^p/\rho$.

in Ref. 29, where more details can be found. As an example in Fig. 29 we show the ratios $\Gamma(3\mathrm{d})/\Gamma(2\mathrm{p},^{16}\mathrm{O})$ for different heavy nuclei, obtained with two standard potentials (with imaginary parts quadratic in density) and the potential derived in [29], which shows saturating properties as the density increases.

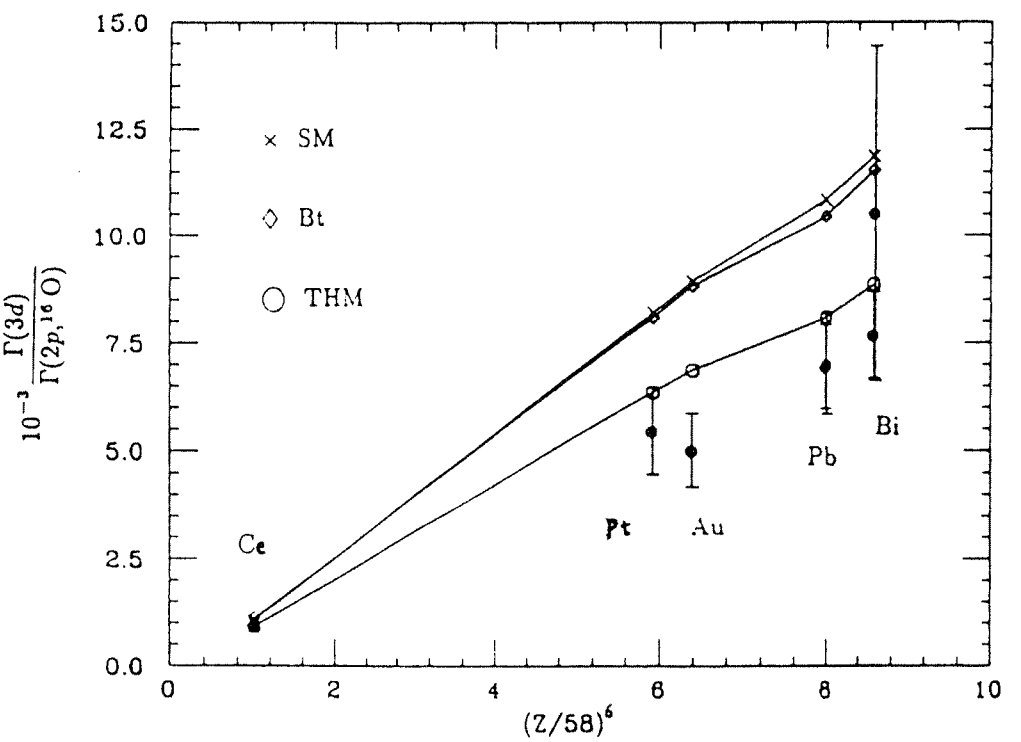

Fig. 29. Ratio $\Gamma(3\mathrm{d})/\Gamma(2\mathrm{p},^{16}\mathrm{O})$ for several heavy nuclei and potentials. SM corresponds to the potential of Ref. 33, Bt to that of Ref. 38 and THM to the theoretical presented here and derived in Ref. 29.

5.3 Low energy pion-nucleus scattering

Consistency of the theoretical approach requires that the extension of the pionic atoms optical potential describes low energy pion (π^-, π^+)-nucleus scattering. In Ref. 30, the potential of Ref. 29 for pionic atoms is extended up to a range of energies of $0 < T_\pi < 50$ MeV. The results are in general quite good, which is even more satisfactory if one takes into account that the model has no free parameters, having been microscopically constructed.

In Fig. 30 we show the center of mass cross section for elastic scattering of 20, 30, 40.2, and 50 MeV π^+ and of 50, 30, and 19.5 MeV π^- from ^{40}Ca, together with the predictions of Ref. 30.

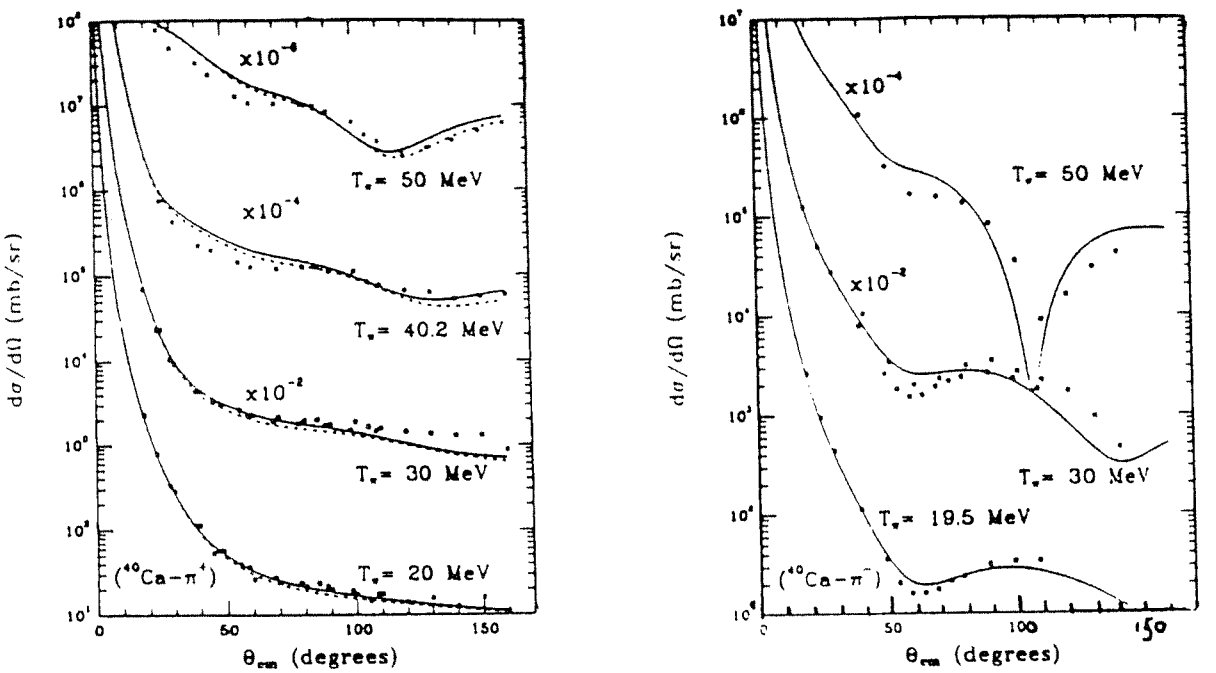

Fig. 30. Center of mass cross section (from [30]) for elastic scattering of $\pi^\pm$ from ^{40}Ca at several pion energies.

The model also allows the separation of the reaction cross section into the quasielastic (incoming pion changes its initial momentum) and absorption (incoming pion is absorbed) channels. The comparison of the results of Ref. 30 for the total reaction (quasielastic plus absorption) cross section and the absorption part for different nuclei and energies is also quite good[24]). In Fig. 31 we present the reaction (R), absorption (A), and quasielastic (Q, the incoming pion changes its initial momentum) cross section for $\pi^\pm$ from ^{197}Au as a function of the kinetic energy of the incoming pion.

The main conclusion of this section is that a many body description of the pion-nucleus interaction is possible in the whole range of intermediate energies[25]). An

[24]) There is no experimental information about the quasielastic channel yet.

[25]) At higher energies, in the Δ resonance region, the model presented here matches the work of Ref. 39 where elastic scattering as well as the different reaction channels: quasielastic, single

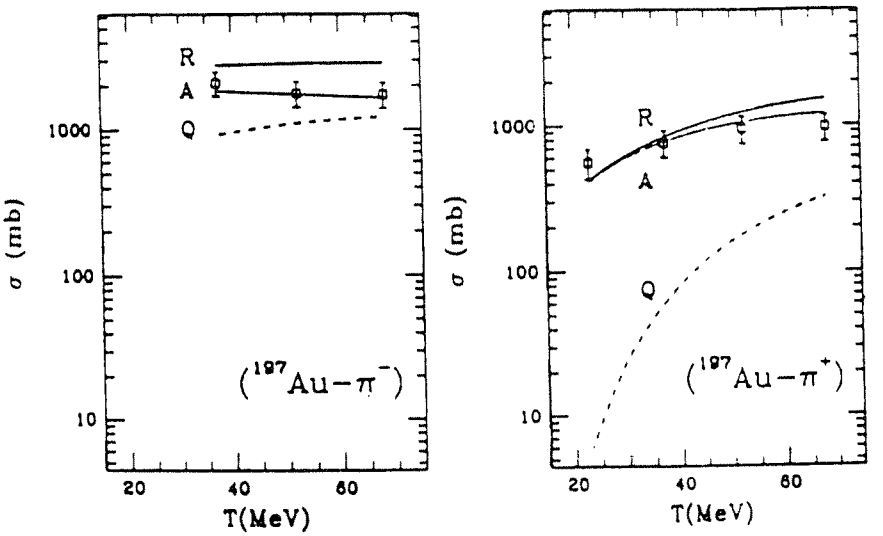

Fig. 31. Reaction (R), absorption (A), and quasielastic (Q) cross section for $\pi^{\pm}$ from ^{197}Au as a function of the kinetic energy of the incoming pion. Results are from [30].

important ingredient to obtain this unified microscopical model has been the proper treatment and inclusion of the medium polarization effects.

6 Mesonic and non-mesonic Λ decay in nuclei[26])

Let us study now the problem of the Λ decay in a nuclear medium. Here, like in the case of the Σ we can also expect an extra decay channel, the ΛN → NN reaction. Note, however, that because there is no strange baryon with smaller mass than the Λ we can not find a reaction which makes the Λ disappear while conserving strangeness, like in the case of the ΣN → ΛN reaction. Thus we are forced to have the ΛN → NN reaction which proceeds via weak interactions. As a consequence the normal Λ → πN decay will not be negligible.

In Fig. 32 we show the Λ self-energy (Σ) diagrams whose imaginary part contribute to the decay width of Λ inside of a nuclear medium. The pion propagation in diagram (a), free decay, gets renormalized inside of the medium, as we saw in the previous sections, and the pion propagator acquires a self-energy. There are two different sources of imaginary part for the Λ self-energy, which correspond to the different cuts shown in Fig. 32: when the intermediate nucleon and the pion are put on shell (pionic decay mode) and when the intermediate nucleon and one intermediate p-h excitation are put on shell (non-mesonic decay mode). In what follows we will study these two different channels, and the role played by the medium corrections on each of them. We will start with the mesonic channel, where we will work directly in finite nuclei instead of in nuclear matter as we have been doing up to now, and we will use the pion-wavefunctions obtained in the previous section to calculate the effect of the medium renormalization in the pionic decay of Λ hypernuclei.

charge exchange, double charge exchange and absorption were fairly well described.

[26]) This section is based on Refs. 21 and 40–42.

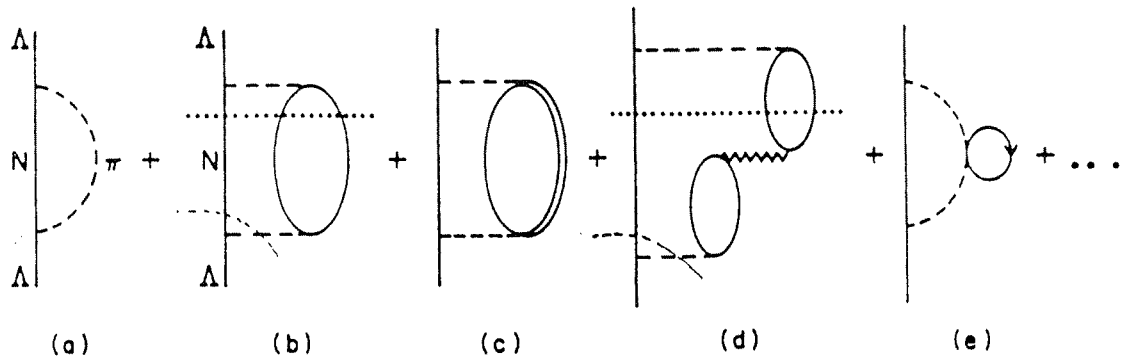

Fig. 32. Λ self-energy diagrams. (a) Free self-energy graph. (b), (c) Insertion of p-wave self-energy at lowest order. (d) Generic RPA graph from the expansion of the pion propagator in powers of the pion self-energy. (e) s-wave self-energy at lowest order.

6.1 Pionic decay of Λ hypernuclei

The mesonic decay of Λ hypernuclei has received attention in the past with most measurements done in emulsion experiments, although some direct measurements are now being performed [43]. At the same time the subject has also received theoretical attention, both in light nuclei and medium and heavy nuclei. One of the peculiar features of the mesonic Λ decay is that the Pauli blocking produces a substantial reduction of the decay width with respect to its free value. On the other hand, another interesting feature of this process is that it is very sensitive to the pion nuclear wave function in the medium. This was first shown in Ref. 42 where the renormalization of the pion in the medium led to large enhancements of the mesonic width. More detailed work by following an alternative method is done in the works of Ref. 44. A thorough work over the periodic table is done in this latter references and the sensitivity to the pion nucleus optical potential is manifestly shown. A review of experimental and theoretical work can be found in Ref. 21.

Here we follow the same method as in [44], to illustrate how the techniques we have learned during these lectures can be also applied to finite nuclei without having to use the local density approximation, and perform a detailed study of the mesonic decay in several nuclei over the periodic table. We will make use of the optical potential pion-nucleus derived microscopically in the previous section.

The widths obtained, measured in units of the free width, range from about 10^{-1} to 10^{-4} from medium to heavy nuclei for decay in π^-p, or $10^{-1} - 10^{-5}$ for decay in π^on.

We start from a Lagrangian for $\Lambda \to \pi$N decay

$$L_{\pi N\Lambda} = G\mu^2 \bar{\psi}_N (A - B\gamma_5)\vec{\tau}\vec{\phi}_\pi \psi_\Lambda + \text{h.c.}, \tag{71}$$

where the terms A and B correspond to the parity violating and parity conserving parts of the interaction respectively. By following [45] ψ_Λ is assumed to behave as the neutron state of an isospin doublet and this implements the $\Delta T = 1/2$ rule by means of which the rate or $\Lambda \to \pi^-$p is twice as large as that of $\Lambda \to \pi^o$n.

Equation 71 leads to an operator in nonrelativistic form of the type

$$H_{\Lambda\pi N} = -G\mu^2 \left[S - \left(\frac{P}{\mu} \right) \vec{\sigma}\vec{q} \right] \tau^{\lambda}, \tag{72}$$

where

$$\begin{aligned} \frac{(G\mu^2)^2}{8\pi} &= 1.945 \times 10^{-15}, \\ S \equiv A &= 1.06, \\ P \equiv \frac{B\mu}{2M} &= 0.527, \end{aligned} \tag{73}$$

and μ and M are the pion and nucleon mass respectively.

The free width is readily evaluated and leads for proton or neutron decay to

$$\Gamma_{\text{free}}^{(\alpha)} = C^{(\alpha)} (G\mu^2)^2 \frac{1}{4\pi} \frac{M q_{\text{cm}}}{M_\Lambda} \left[S^2 + \left(\frac{P}{\mu} \right)^2 q_{\text{cm}}^2 \right], \tag{74}$$

$$q_{\text{cm}} = \frac{\lambda^{1/2}(M_\Lambda^2, M^2, \mu^2)}{2M_\Lambda}, \quad C^{(\text{p})} = 4, \quad C^{(\text{n})} = 2,$$

with M_Λ the Λ mass and q_{cm} the pion momentum in the center of mass frame. One can see from Eq. 74 that the parity violating term is the dominant one in the decay.

In the first place we observe that, if one were to compute the Λ decay inside of nuclear matter, one would get a Pauli blocking factor of the type $1 - n(\vec{k} - \vec{q})$, with $\vec{k}$ and $\vec{q}$ the Λ and nucleon momenta, which will ensure that the outgoing nucleon cannot go to an occupied state. Since a Λ with $\vec{k} = 0$ decays into a nucleon and pion with $q \approx 100\,\text{MeV}/c$ (energy-momentum conservation), this momentum is smaller than the Fermi momentum for normal nuclear matter density, $k_{\text{F}} = 270\,\text{MeV}/c$ and the decay is forbidden by Pauli blocking, i.e., $1 - n(\vec{k} - \vec{q}) = 0$. The overlap of the Λ wave function with the nuclear surface in finite nuclei still allows the Λ decay since at some radius the local Fermi momentum will be smaller than $100\,\text{MeV}/c$, and also because the momentum distribution of the Λ wave function helps a bit in allowing some nucleon momenta in the decay. Nevertheless the Λ mesonic width decreases drastically as a function of the mass number.

There is another important fact which makes weaker the effect of the Pauli blocking. The pion propagation in a nuclear medium is modified with respect to its propagation in the vacuum. The pion gets a self-energy in nuclear matter, or equivalently it propagates under the action of an optical potential pion-nucleus in finite nucleus. In nuclear matter, the attractive character of the pion self-energy[27]) leads to a larger pion momentum for the same pion energy and thus, to a larger nucleon momentum by momentum conservation. Thus, the nucleon has more chances to have a momentum bigger than the Fermi momentum, therefore increasing the width.

[27]) Above threshold, the p-wave, which is attractive, is the dominant part in the pion self-energy, while the s-wave contribution is just a small fraction of it.

The width for the Λ decay inside a nucleus is given by [40]

$$\Gamma^{(\alpha)} = \frac{1}{2} C^{(\alpha)} \sum_{\mathrm{N} \neq \mathrm{F}} \int \frac{\mathrm{d}^3 q}{(2\pi)^3} \frac{1}{2\omega(q)} 2\pi \delta(E_\Lambda - \omega(q) - E_\mathrm{N}) (G\mu^2)^2$$
$$\times \left[S^2 \left| \int \mathrm{d}^3 x \varphi_\Lambda(\vec{x}) \widetilde{\varphi}_\pi^{(-)}(\vec{q}, \vec{x})^* \varphi_\mathrm{N}^*(\vec{x}) \right|^2 \right.$$
$$\left. + \left(\frac{P}{\mu} \right)^2 \left| \int \mathrm{d}^3 x \varphi_\Lambda(\vec{x}) \vec{\nabla} \widetilde{\varphi}_\pi^{(-)}(\vec{q}, \vec{x})^* \varphi_\mathrm{N}^*(x) \right|^2 \right], \qquad (75)$$

where $\varphi_\mathrm{N}, \varphi_\Lambda$ are the nucleon and lambda wave functions, E_N and E_Λ their corresponding energies, $\omega(q)$ the pion energy, and the sum over N runs over the unoccupied orbitals n, l since spin sums are already performed. Hence we do not consider the spin orbit splitting of the levels and work in an l, s basis for the nuclear excited states. In Eq. 75 and in what follows the sums over N are over proton or neutron orbitals according to α.

The pion wave function $(\widetilde{\varphi}_\pi^{(-)}(\vec{q}, x)^*)$ as a block corresponds to an incoming solution of the Klein-Gordon equation

$$[-\vec{\nabla}^2 + \mu^2 + 2\omega V_\mathrm{opt}(\vec{x})] \, \widetilde{\varphi}_\pi^{(-)}(\vec{q}, \vec{x})^* = (\omega - V_\mathrm{C}(\vec{x}))^2 \, \widetilde{\varphi}_\pi^{(-)}(\vec{q}, \vec{x})^* \,, \qquad (76)$$

with $V_\mathrm{C}(\vec{x})$ the Coulomb potential created by the nucleus considering finite size effects and V_opt the optical potential pion-nucleus derived in the previous section. One can see that

$$\widetilde{\varphi}_\pi^{(-)}(\vec{q}, \vec{x})^* \equiv \varphi_\pi^{(+)}(-\vec{q}, \vec{x}) \,, \qquad (77)$$

where $\varphi_\pi^{(+)}(-\vec{q}, \vec{x})$ corresponds to an incoming solution for a pion of momentum $-\vec{q}$.

The use of Eq. 77 for the outgoing pion wave function guarantees that pion flux is lost to the reaction channels, (accounted for by the imaginary part of the complex optical potential), when the pions move out through the nucleus.

In finite nuclei, the argument for the effect of the pion renormalization (change of plane wave for the outgoing pion by a solution of the Klein-Gordon equation with a proper potential in Eq. 75) is expressed now in the alternative language as follows: the attraction caused by the pion-nucleus optical potential increases the pion momenta in the pion wave function. As a consequence the matrix element of the Λ wave function (in a $1s_{1/2}$ ground state of the Λ nucleus potential) and the nucleon wave function is considerably enhanced. Note that if the Λ and N potentials were the same, the Λ and the nucleon states above the Fermi sea are orthogonal and the matrix elements of Eq. 75 would be zero for $\vec{q} = 0$. The matrix elements thus necessarily increase with $\vec{q}$, for the moderately small values of $\vec{q}$ involved in the present process. In the two languages (nuclear matter or finite nuclei) the physical consequences are the same: an increased probability of reaching the unoccupied states and thus an enhancement of the mesonic width in about two orders of magnitude in heavy nuclei, as we will see.

Now we are in condition to evaluate Eq. 75 and obtain thus the pionic decay widths of Λ hypernuclei. The only detail still missing is the calculation of the Λ and nucleon wave-functions. In [40], whose results we will show here, shell model potentials were used both for the Λ particles and the nucleons. For the Λ, a potential was taken (in MeV)

$$V(r) = -32\frac{\rho(r)}{\rho_0}, \tag{78}$$

where $\rho(r)$ is the nuclear density and $\rho_0 \equiv \rho(r=0)$, and for the nucleons

$$\begin{aligned} V(r) &= -50\, f(r), \\ f(r) &= \frac{1}{1+\exp\left[(r-R)/a\right]}, \end{aligned} \tag{79}$$

with $R = 1.25\ A^{1/3}$ fm, $a = 0.65$ fm, which provides a fair reproduction of the nuclear levels for the average energy of major shells, as well as realistic nucleon wave functions.

In Ref. 40 one can find abundant results in different nuclei which are rather realistic. Some details which have been omitted here, as the accurate description of the energy balance in the particular reactions, transitions to the bound and continuum N states and the separation of the pion-nucleus optical potential imaginary part into two terms related to pion absorption and quasielastic scattering[28]) can be found there.

In Fig. 33 we show the prediction of Ref. 40 for different nuclei and for π^0 and π^- decay, with plane waves and the renormalized pion wave function. The drastic effects of the pion renormalization are seen there and are a bit smaller than in former works because the energy balance makes the pions come out with smaller energies than in the previous approaches and the attractive effects of the p-wave part of the optical potential are then diminished.

Of particular relevance are the results in ${}^{12}_{\Lambda}$C. One obtains the results shown in Table 2.

Although with large errors, the experimental results confirm these striking theoretical predictions which show a large violation of the $\Delta T = 1/2$ in nuclei ($\Gamma_{\pi^0}/\Gamma_{\pi^-}$ should be 0.5 under this rule) due mostly to nuclear shell effects.

Another interesting finding is seen in very light nuclei. The mesonic width of ${}^{5}_{\Lambda}$He has attracted particular attention. There, in addition to the pion renormalization, the repulsive character of the ΛN interaction and the relatively weaker medium range attraction, compared to the NN interaction, has as an effect pushing the Λ to

[28]) In [40] pion quasielastic events are not removed from the pion flux, as it corresponds to the actual experimental observation, while the use of a full distortion of the pion with the total optical potential, as done in [44], inevitably removes the pion quasielastic events, together with the pion absorption events. Though conceptually important, this refinement turns out to be of little practical relevance in the present problem given the small energy that the pions carry and the very small phase space for quasielastic collisions. However, other considerations, particularly the energy balance in the reactions makes the widths in heavy nuclei for π^--decay about one order of magnitude smaller than those of Ref. 44.

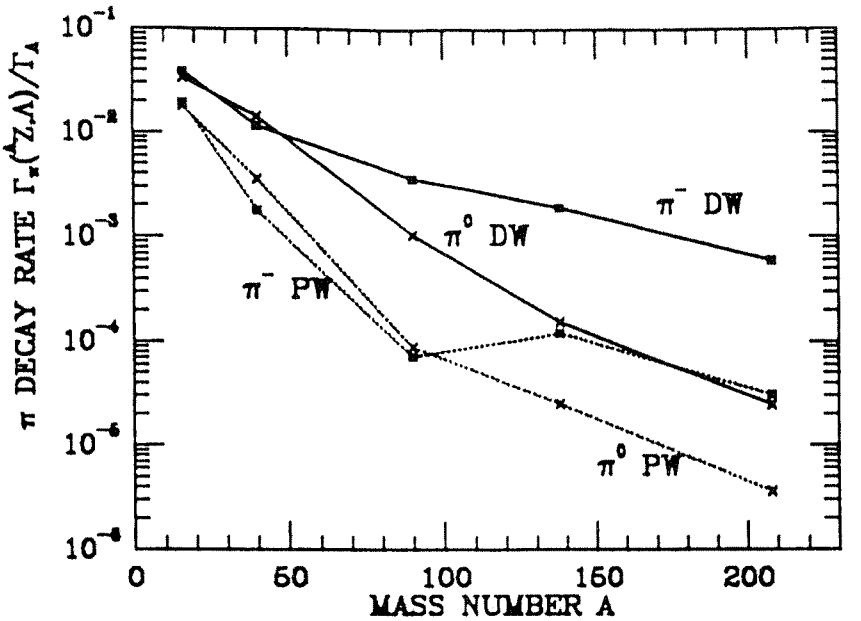

Fig. 33. Pionic decay rate for π^0 and π^- as a function of the mass number (of the host nucleus, ^{16}O, ^{40}Ca, ^{90}Zr, ^{138}Ba, and ^{208}Pb), from Ref. 40. The two lower lines show the calculation with plane waves for the pion and the two upper lines the results with pion distorted waves.

Table 2.

	$\Gamma_{\pi^0}/\Gamma_\Lambda$	$\Gamma_{\pi^-}/\Gamma_\Lambda$	$\Gamma_{\pi^0}/\Gamma_{\pi^-}$
Ref. 40	0.159	0.086	1.86
Ref. 44	0.13	0.098	1.32
Exp.	0.217 ± 0.084	$0.052 \pm^{0.063}_{0.035}$	

the surface of the nucleus, weakening the Pauli blocking effect and thus enhancing the mesonic decay [46]. The experimental numbers clearly favour potentials with a repulsive ΛN core. One should note that such a repulsion automatically appears in quark based models of the ΛN interaction. A recent study of the $^{5}_{\Lambda}$He decay using a quark model based hypernuclear wave function [47] leads to the results shown in Table 3.

Table 3.

	$\Gamma_{\pi^-}/\Gamma_\Lambda$	$\Gamma_{\pi^0}/\Gamma_\Lambda$	$\Gamma_{\rm tot}/\Gamma_\Lambda$
Ref. 47	0.431	0.239	0.670
Exp.	0.44 ± 0.11	0.18 ± 0.20	$0.59 \pm^{0.44}_{0.31}$

These theoretical results are also in good agreement with those of Ref. 48 when a Λ wave function from the modified YNG ΛN interaction of Ref. 49, which has a strong repulsion at short distances is used.

6.2 Non-mesonic Λ decay in nuclei

Let us now turn our attention to the non mesonic decay. As we discussed above, one gets this contribution when for instance in diagram (b) of Fig. 32 the intermediate nucleon and the p-h excitation are put on shell. However, note that in this way, we would have only one pion exchange as responsible for the $\Lambda N \to NN$ transition. It is clear that we could have other ingredients as well, since now we have exchange of virtual particles. Different approaches have been taken: $\pi + \rho$ exchange [50], pion exchange modified at short distances by new forces appearing when the two quarks bags overlap [51], π, ρ, K, K*, ω, ... and short distance correlations ΛN [52], etc. ...

Furthermore, we can also have Λ decay induced by pairs of nucleons leading to a three nucleon decay channel $\Lambda NN \to NNN$ [53].

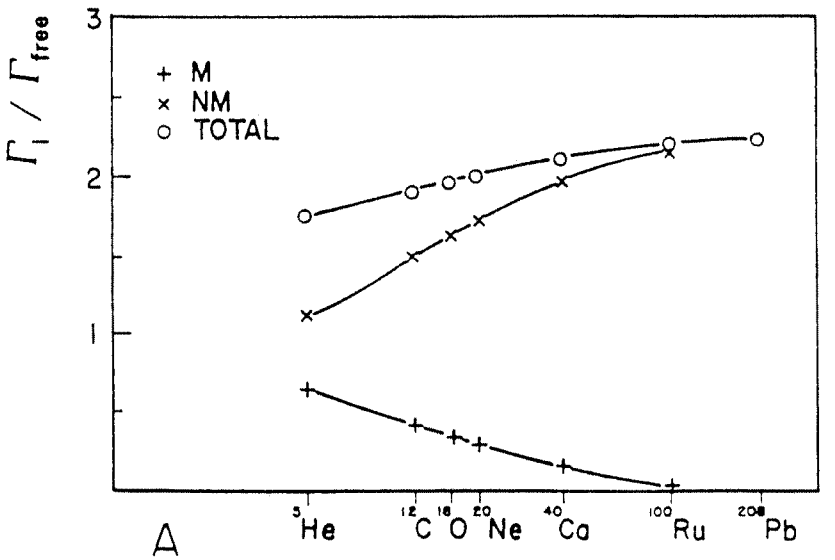

Fig. 34. Mesonic and non mesonic Λ width as a function of the atomic number.

Thus, the subject is at the moment the object of an intense activity by several groups and we will limit our discussion here to a qualitative level. We just mention that the non-mesonic decay is the dominant mode for decay of Λ hypernuclei and that it can be as large as twice the free decay width for heavy nuclei. To illustrate this in Fig. 34, which should be considered merely at a qualitative level, we plot the result for Γ_M (pionic mode) and Γ_{NM} (non-mesonic mode) from Ref. 42 for different nuclei, where we observe that for heavy nuclei $\Gamma/\Gamma_{\text{free}}$, $\Gamma = \Gamma_M + \Gamma_{NM}$ is around 2 and Γ_M decreases gradually as the atomic number increases.

7 Conclusions

We have studied different problems of Nuclear Physics, apparently disconnected, but with a common link in their sensitivity to the spin-isospin part of the baryon-baryon interaction and to the peculiar way that this interaction is modified in a nuclear medium. We have reviewed the problem of the muon capture in nuclei, the

nature and decay modes of Σ and Λ hypernuclei and finally we have addressed the main features of the pion-nucleus interaction at low energies. The framework to deal with these problems has been Many Body Quantum Field Theory, which proves to be an ideal method to calculate efficiently and reliably most nuclear magnitudes, and which offers, through its diagramatic method, an intuitive picture of the physical meaning of the magnitudes which are calculated.

Many other topics could have also been included, photo- and electro-nuclear reactions, scattering K^+-nucleus, $\bar{p}$ annihilation in nuclei... with similar conclusions and success, but for reasons of space have not been considered here.

I would like to acknowledge the essential contributions of most of my colleagues from the group of Prof. E. Oset. In particular, I am in debt with E. Oset, C. García-Recio, M.J. Vicente-Vacas, H.C. Chiang, L.L. Salcedo, P. Fernández de Cořdoba and many others... who have helped me to understand the techniques of Many Body Quantum Theory and the main features of the different physical processes presented in these lectures. I would also like to thank the Organizing Committee and in particular J. Adam and P. Bydžovský for all their dedication, support and help during the celebration of this School.

References

[1] Fetter A.L. and Walecka J.D.: Quantum Theory on Many Particle Systems. McGraw-Hill, New York, 1971.

[2] Mattuck R.D.: A guide to Feynman Diagrams in the Many-Body Problem. McGraw-Hill, New York, 1974.

[3] Oset E.: *in* Quarks, Mesons and Isobars (ed. R. Guardiola and A. Polls). World Scientific, Singapore, 1983 p. 1.

[4] Oset E.: *in* the SERC School of Nuclear Physics, Jaipur, India 1987 (ed. B.K. Jain). World Scientific, Singapore, 1987.

[5] Mandl F. and Shaw G.: Quantum Field Theory. John Wiley, New York, 1984.

[6] Itzykson C. and Zuber J.B.: Quantum Field Theory. McGraw-Hill, New York 1983.

[7] Oset E., Toki H., and Weise W.: Phys. Rep. *83* (1982) 281.

[8] Ericson M.: Nucl. Phys. A *335* (1980) 309.

[9] Bjorken J.D. and Drell S.D.: Relativistic quantum fields. McGraw-Hill, New York, 1965.

[10] Alberico W., Ericson M., and Molinari A.: Nucl. Phys. A *379* (1982) 429.

[11] Oka M. and Yazaki K.: Phys. Lett. B *90* (1980) 41.

[12] Faessler A., Fernandez F., and Lübec G.: Phys. Lett. B *112* (1982) 201.

[13] Holinde K.: Phys. Rep. *68* (1981) 121.

[14] Brown G.E. and Jackson J.D.: The Nucleon Nucleon Interaction. North Holland, Amsterdam, 1979.

[15] Brown G.E.: Many Body Problems. North Holland, Amsterdam, 1972.

[16] Chiang H.C., Oset E., and Fernández de Córdoba P.: Nucl. Phys. A *510* (1990) 591.

[17] Primakoff H.: Rev. Mod. Phys. *31* (1959) 802.

[18] Blin-Stoyle R.J.: Fundamental Interactions and the Nucleus. North-Holland, Amsterdam, 1973.

[19] Mukhopadhyay N.C.: Phys. Rep. *30* (1977) 1.

[20] Navarro J., Bernabeu J., Gómez J.M.G., and Martorell J.: Nucl. Phys. A *375* (1987) 361.

[21] Oset E., Fernández de Córdoba P., Salcedo L.L., and Brockmann R.: Phys. Rep. *188* (1990) 79.

[22] Batty C.J. et al.: Phys. Lett. B *74* (1978) 27.

[23] Bertini R. et al.: Phys. Lett. B *90* (1980) 375; *136* (1984) 29; *158* (1985) 19.

[24] Hayano R.S.: Nucl. Phys. A *478* (1988) 113c.
Hayano R.S. et al.: Phys. Lett. B *231* (1989) 235.

[25] Bando H., Motoba T., and Zofka J.: Z. Phys. A *330* (1988) 203.

[26] Brockman R. and Oset E.: Phys. Lett. B *118* (1982) 33.

[27] Nagels M.M., Ryken T.A., and de Swart J.J.: Phys. Rev. D *15* (1977) 2547; *20* (1979) 1633.

[28] Brockman R. and Oset E.: Nucl. Phys. A *450* (1986) 353c.

[29] Nieves J., Oset E., and García Recio C.: Nucl. Phys. A *554* (1993) 509.

[30] Nieves J., Oset E., and García Recio C.: Nucl. Phys. A *554* (1993) 554.

[31] Ericson T. and Weise W.: Pions and Nuclei. Oxford University Press, 1988.

[32] Ericson M. and Ericson T.E.O.: Ann. Phys. *36* (1966) 323.

[33] Seki R. and Masutani K.: Phys. Rev. C *27* (1983) 2799.

[34] Seki R.: *in* Pion-nucleus physics: future directions and new facilities at LAMPF, A.I.P. Conf. Proc., Vol. 163 (ed. R.J. Peterson and D.D. Strottman). AIP, New York, 1988, p. 233.

[35] Konijn J., de Laat C.T.A.M., Taal A., and Koch J.H.: Nucl. Phys. A *519* (1990) 773.

[36] Seki R., Masutani K., and Toki H.: Phys. Lett. B *263* (1991) 1.

[37] García-Recio C., Oset E., and Salcedo L.L.: Phys. Rev. C *37* (1988) 194.

[38] Batty C.J. et al.: Nucl. Phys. A *322* (1979) 445.

[39] García-Recio C., Oset E., Salcedo L.L., Strottman D., and López M.J.: Nucl. Phys. A *526* (1991) 685.
Salcedo L.L., Oset E., Vicente-Vacas M.J., and García-Recio C.: Nucl. Phys. A *484* (1988) 557.

[40] Nieves J. and Oset E.: Phys. Rev. C *47* (1993) 1478.

[41] Oset E., Fernández de Córdoba P., Nieves J., Ramos A., and Salcedo L.L.: Prog. Theor. Phys. Suppl. *177* (1994) 461.

[42] Oset E. and Salcedo L.L.: Nucl. Phys. A *443* (1985) 704.

[43] Grace R. et al.: Phys. Rev. Lett. *55* (1985) 1055.
Sakaguchi A. et al.: Nuovo Cimento *102A* (1989) 511.
Barnes P.D.: Nucl. Phys. A *450* (1986) 43c; *478* (1988) 127c.
Szymanski J.J. et al.: Phys. Rev. C *43* (1991) 849.

[44] Itonaga K., Motoba T., and Bando H.: Z. Phys. A *330* (1988) 209.
Motoba T., Itonaga K., and Bando H.: Nucl. Phys. A *489* (1988) 683.
Motoba T.: Nucl. Phys. A *527* (1991) 485c; Few Body Systems, Suppl. *5* (1992) 386; *in* Proc. International Symp. on Hypernuclear and Strange Particle Physics, Shimoda 1991 – Nucl. Phys. A *547* (1992) 115c.

[45] McKellar B.H.J and Gibson B.F.: Phys. Rev. C *30* (1984) 322.

[46] Kurihara Y., Akaishi Y., and Tanaka H.: Phys. Rev. C *31* (1985) 971.
Oset E., Salcedo L.L., and Usmani Q.N.: Nucl. Phys. A *450* (1986) 67c.

[47] Straub U., Nieves J., Faessler A., and Oset E.: Nucl. Phys. A *556* (1993) 531.

[48] Motoba T., Bando H., Fukuda T., and Žofka J.: Nucl. Phys. A *534* (1991) 597.

[49] Yamamoto Y. and Bando H.: Prog. Theor. Phys. *73* (1985) 905; Prog. Theor. Phys. Suppl. *81* (1985).

[50] McKellar B.H.J. and Gibson B.F.: Phys. Rev. C *30* (1984) 322.

[51] Cheung C.Y., Heddle D.P., and Kisslinger L.S.: Phys. Rev. C *27* (1983) 355.

[52] Benhold C. and Ramos A.: Nucl. Phys. A *585* (1995) 373c.

[53] Ramos A., Oset E., and Salcedo L.L.: Phys. Rev. C *50* (1994) 2314.